

Novel Control-Oriented Models for Liquid Transport in Falling Film Evaporator Tubes

Anton Ponomarev^{a,*}, Julian Hofmann^b, Lutz Gröll^b

^aSaint Petersburg State University, Department of Mechanics of Controlled Motion, Universitetskaya nab. 7/9, St. Petersburg 199034, Russia

^bKarlsruhe Institute of Technology, Institute for Automation and Applied Informatics, Hermann-von-Helmholtz-Platz 1, Eggenstein-Leopoldshafen 76344, Germany

A B S T R A C T

The paper presents novel control-oriented transport models for evaporating liquid films in the tubes of a falling film evaporator. In this context, our goal consists in qualitatively mapping the experimentally observed input-output behavior. Two transport models are proposed, where the difference between them is that one allows overtaking of liquid particles and the other does not. The transport models are equipped with two new models of evaporation which are different from the commonly assumed uniform evaporation. The models are initially developed from the conservation laws in the form of partial differential equations. Using the method of characteristics we then obtain the input-output relations for the proposed models in the form of time-delay equations. The time-delay representation is advantageous for simulation and for the future control design. In a simulation study, we observe the principal properties of the models and find that they correspond well with the experimentally observed input-output behavior.

Keywords:

transport model
liquid film
input-output behavior
partial differential equation
time-delay equation
falling film evaporator

1. Introduction

In numerous chemical engineering applications, such as vessels Zenger and Ylinen (1994), reactors Levenspiel (1999), mixers Niemi (1977), substances in soils Misra and Mishra (1977), heat exchangers Maida et al. (2009) or falling film evaporators Winchester (2000), the modeling of transport processes is of basic interest. To describe the transport mathematically, there are two options: PDEs and time-delay equations.

The PDE-based approach commonly uses fundamental balance equations of mass, momentum and energy, which form the basis for various kinds of transport Grifoll et al. (2005); Van Genuchten (1982); Zhang (1998); Zheng and Bennett (2002). Time-delay equations, on the other hand, are often phenomenologically motivated Cascetta (2013) and are based on the continuity equation of, e.g., liquid elements, such as plugs Kicsiny (2014); Niemi (1977); Zenger and Ylinen (1994).

The relation between PDE and time-delay models was investigated by Karafyllis and Krstic (2014, 2020). While the focus of Karafyllis and Krstic (2014, 2020) is on system-theoretic aspects

of the two kinds of models, the present research is motivated by the control-oriented advantages of the *time-delay* representations: they enjoy a wider range of common analysis techniques and control algorithms, including adaptive ones Evesque et al. (2003); Zhong (2006), and are easier to implement in full-plant simulations in the environments such as Simulink where time-delay blocks are standard.

Herein, we adopt the methodology which consists in deriving fundamentally motivated PDE models that are subsequently approximated by or transformed into time-delay equations. Prior examples of this constructive approach are found in Bresch-Pietri and Petit (2016); Bresch-Pietri et al. (2013); Diagne et al. (2013); Rodriguez et al. (2016); Witrant and Niculescu (2010) but they do not suitably describe the complexity of our process as is explained next.

Our practical application is the FFE process GEA Wiegand GmbH (2016) where two types of transport dynamics are crucial: the flow of liquid through completely filled *pipes* and the flow of evaporating liquid film down the sides of partially filled *tubes* Paramalingam (2004); Schwaer et al. (2020); Winchester (2000). The flow through the pipes is the easier case where the density, concentration or temperature transport can be well described by classical transport models with time-varying velocity Bresch-Pietri and Petit (2016); Dobos et al. (2009); Rodriguez et al. (2016); Zenger and Ylinen (1994). As for the transport of evaporating falling films, it is often modeled by assuming that *velocity* is

Abbreviations: FFE, falling film evaporator; PDE, partial differential equation; IC, initial condition; BC, boundary condition; i/o, input-output; DPF, dynamic plug flow; OPF, overtaking particle flow.

* Corresponding author.

E-mail address: anton.pon.math@gmail.com (A. Ponomarev).

constant and evaporation is uniformly distributed along the tubes Bojnourd et al. (2015); Paramalingam (2004); Quaak et al. (1994); Stefanov and Hoo (2003); Winchester and Marsh (1999). In reality, though, the velocity of liquid films depends on time-varying quantities, such as mass flow, density or viscosity Craster and Matar (2009), which causes *time-varying* transport delays of the liquid elements in the tubes. Moreover, there are wave phenomena which essentially influence the dynamics of the liquid film and lead to accumulations of liquid elements at different points in the tubes Albert et al. (2014); Bandi et al. (2018); Ruyer-Quil and Manneville (2000). Therefore, the aforementioned transport models are only rough approximations of the real behavior.

To model more realistic behavior of the evaporating falling film, there exist computational fluid dynamics simulations which are based on coupled Navier-Stokes equations for liquid and vapor phase Donaldson and Thimmaiah (2016); Kharangate et al. (2015). However, such detailed models as in Albert et al. (2014); Bandi et al. (2018); Kharangate et al. (2015); Ruyer-Quil and Manneville (2000) are too complex for control design and hard to embed in full plant simulations.

Therefore, we develop two novel transport models based on fundamental balance equations. Apart from liquid films, they can be applied to other transport processes that satisfy certain assumptions. The models and their characteristic features can be described as follows:

1. *Dynamic Plug Flow (DPF)*: Transported instances, e.g., liquid elements, move without overtaking such that the First-In-First-Out (FIFO) principle holds. The instances may have different velocities but the velocity of a single instance stays constant during its travel.
2. *Overtaking Particle Flow (OPF)*: The instances can overtake one another. At the input they assume different velocities according to a probability-like distribution function but still, each instance's velocity stays constant during its travel.

Both models are able to show advanced dynamic effects, such as wave phenomena or time-varying residence times. Furthermore, the second model (OPF) has the remarkable property of modeling diffusion without the commonly used second-order spatial derivative term in the PDE which is achieved by assigning different velocities to the incoming instances.

The DPF and OPF transport models were originally introduced in Hofmann et al. (2020). This paper differs in that here we consider evaporation from the falling film, the contribution being as follows. Since the assumption of uniform evaporation (the total vapor mass flow from the tube is distributed uniformly among the liquid flow elements), as applied in Bojnourd et al. (2015); Paramalingam (2004); Quaak et al. (1994); Stefanov and Hoo (2003); Winchester and Marsh (1999), may prove disadvantageous as explained later in the paper, we present two new approaches to model evaporation:

1. *Water-proportional* evaporation model where the total vapor mass flow from the tube is distributed among the liquid flow elements proportionally to the water content of the element.
2. *Localized* evaporation model where vapor mass flow from each liquid element is calculated separately.

Uniting the transport and evaporation models, for technical reasons mentioned later we limit our attention to the following four combinations:

1. DPF with uniform evaporation.
2. DPF with water-proportional evaporation.
3. OPF with water-proportional evaporation.
4. OPF with localized evaporation.

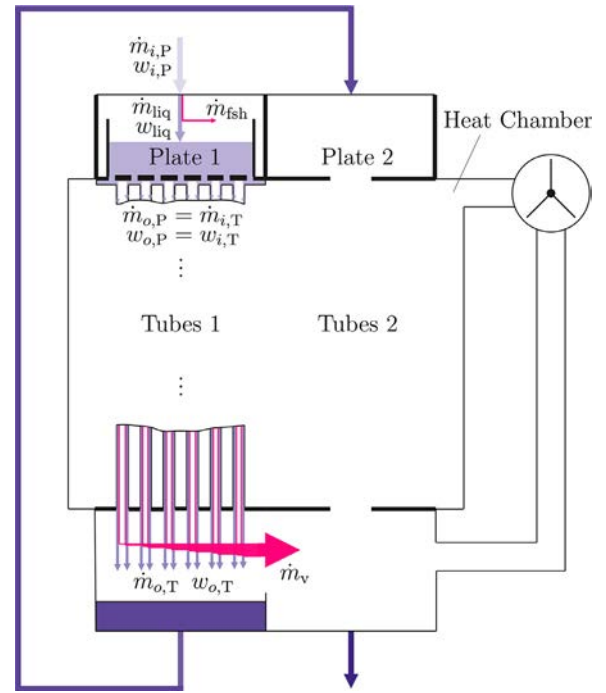


Fig. 1. Scheme of an FFE with two passes, each consisting of Plate and Tubes. While the first pass is visualized in detail, the second one is roughly sketched.

The models are first constructed in the form of a system of PDEs with boundary inputs and outputs. Since the PDE models are hyperbolic, we apply the method of characteristics Courant and Hilbert (1989); Sarra (2003) to obtain the corresponding time-delay i/o relations. The latter are advantageous for simulation and control design Bresch-Pietri and Petit (2016); Rodriguez et al. (2016); Witrant and Niculescu (2010). Although this contribution focuses on transport models for evaporating liquid films, our results may also be applied to other transport processes, e.g., in traffic flow Daganzo (1994); Čičić and Johansson (2018); Zhang (1998) which can be motivated via analogies.

The plan of the paper is as follows. In Sec. 2, the falling film evaporator process is specified and motivated as a technical application of our models. Two novel models of evaporating liquid films, DPF and OPF, are introduced in Sec. 3 and Sec. 4, respectively. Each model is first explained in the general terms (Sec. 3.1 and 4.1), then derived as a system of PDEs (Sec. 3.2 and 4.2) and subsequently, under certain evaporation assumptions, transformed into time-delay i/o equations (Sec. 3.3, 3.4, 4.3 and 4.4). Section 5 shows the results of simulation of our new models and discusses their ability to map the observed qualitative i/o behavior. In Sec. 6, we sum up the results.

2. Preliminaries

In this section we describe the falling film evaporator and recall some formulas that will be used in the subsequent constructions.

2.1. Falling Film Evaporator: Process Description

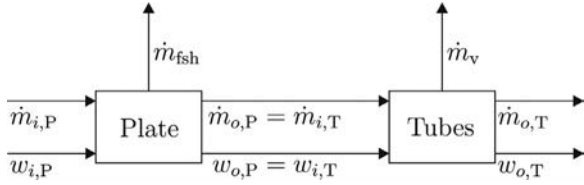
FFEs are industrial heat exchangers. They are often applied in the food, pharmaceutical or chemical industry to concentrate liquid temperature-sensitive products, such as milk, orange juice, coffee, drugs or bio-ethanol. The flow capacity of these plants is up to 150 tons per hour, see GEA Wiegand GmbH (2016).

Figure 1 shows the scheme of a two-pass FFE. Raw product (water-based solution of some useful material), is pumped onto the

Table 1

Symbol and subscript nomenclature.

Symbols	Units
A	cross-sectional area m^2
c	velocity $m s^{-1}$
c_p	specific heat capacity $J kg^{-1} K^{-1}$
d	inner diameter of tubes m
g	gravity acceleration $m s^{-2}$
h	filling level m
Δh_v	enthalpy of evaporation $J kg^{-1}$
k	heat transfer coefficient $W m^{-2} K^{-1}$
ℓ	length of tubes m
\dot{m}	mass flow $kg s^{-1}$
M	mass kg
n	number of tubes in pass $-$
Re	Reynolds number $-$
s	film thickness m
w	dry matter content $kg kg^{-1}$
η	dynamic viscosity $kg m^{-1} s^{-1}$
ϑ	temperature K
ϱ	volumetric mass density $kg m^{-3}$
τ	time delay s
Subscripts	
0	initial value
d	dry matter
fsh	flash evaporation
h	homogeneous
H	heat chamber
i	input
max	maximum
min	minimum
o	output
O	orifices in plate tank
p	particular
P	plate
R	ring
T	tubes
v	vapor
w	water

**Fig. 2.** Flow diagram of an FFE pass

first distribution plate (Plate 1). From there it falls down the narrow vertical Tubes 1, uniformly covering their inner walls as a thin “falling film”. The tubes are heated from the outside by hot water vapor coming from the Heat Chamber which causes some water content to evaporate from the film. The vapor is sucked out by the compressor into the Heat Chamber and repurposed for heating the tubes. Meanwhile, the intermediate product coming out of Tubes 1 drops into a reservoir, is transported onto Plate 2 and undergoes the similar second pass through Tubes 2, turning into the final concentrated product. In each pass, the concentration increases, while being limited by viscosity constraints. If viscosity becomes too high, deposits on the tube walls cause undesired fouling Díaz-Ovalle et al. (2017).

The nomenclature of symbols and subscripts used throughout the paper is shown in Table 1.

2.2. FFE Pass Model

Figure 2 depicts the flow diagram of an FFE pass. For the Plate block, we borrow the model from Schwaer et al. (2020) which is essentially a low-pass filter whose time constant depends on the operation point. Additionally, there is a small mass flow \dot{m}_{fsh}

which evaporates from the liquid when it enters the Plate and thus undergoes a fast reduction in pressure Paramalingam (2004). In Sections 3 and 4 we develop novel transport models for the Tubes block: the so-called DPF and OPF models.

In order to assess the quality of our models, we will compare them qualitatively to the i/o behavior of one FFE pass which is observed in practice. The behavior is illustrated by Fig. 3 where changes in the output mass flow and dry matter content are shown in response to an up/down-step in the input mass flow while evaporation mass flow and input dry matter content are kept constant. In case of an up-step, we expect a delay in the response of the output mass flow with some overshoot. In case of a down-step, there is also a delayed response. The overshoot is caused by wave-like effects Bandi et al. (2018); Albert et al. (2014). Regarding dry matter content, the delay is similar to that of the output mass flow. Since larger input mass flow causes larger transport velocity and shorter residence of liquid inside the tube, it leads to less evaporation which can be concluded from both the mass flow and dry matter content plots.

To justify the qualitative i/o behavior in Fig. 3, we present data from an up-step experiment in a one-tube pilot plant with water and constant evaporation, see Fig. 3. As no direct measurement of $\dot{m}_{o,T}$ is available, we calculate it via numerical differentiation of the water level in the reservoir after the tube and, to this end, basic moving average filter is used (Hofmann et al., 2021). In this experiment, we observe both the delayed response and the overshoot.

2.3. Average Film Velocity at the Tube's Inlet

The average film velocity at the inlet of the evaporator tubes $\bar{c}_{i,T}$ will be used in the boundary conditions of the PDEs. Here we derive the formula for $\bar{c}_{i,T}$ via the average film thickness denoted \bar{s} .

The film's cross-sectional area, combined over n tubes in one pass, is $A_R = \pi n(d - \bar{s})\bar{s}$ and the input mass flow into the tubes is $\dot{m}_{i,T} = \varrho \bar{c}_{i,T} A_R$. Thus, we find

$$\bar{c}_{i,T} = \frac{\dot{m}_{i,T}}{\varrho \pi n (d - \bar{s}) \bar{s}}. \quad (1)$$

There exist numerous correlations Åkesjö (2018); Lukach et al. (1972); Martin et al. (2002) to determine the average film thickness \bar{s} . In this paper, the formula

$$\bar{s} = \left(\frac{3\eta^2}{g\varrho^2} Re \right)^{1/3}, \quad Re = \frac{\dot{m}_{i,T}}{\eta \pi d n} \quad (2)$$

is applied which was developed by Nusselt Nusselt (1916) for stationary laminar flow.

As $\dot{m}_{i,T}$, ϱ and η can vary with time, time-varying quantities $\bar{c}_{i,T}(t)$, $\dot{m}_{i,T}(t)$, $\varrho(t)$ and $\bar{s}(t)$ are formally substituted in (1).

3. First Transport Model: Dynamic Plug Flow (DPF)

3.1. General Principles of the Model

Fig. 4 serves as a kinematic diagram of the DPF transport model. For convenience, water/dry content separation and evaporation is disregarded in Fig. 4. The model is based on the following assumptions:

1. Particles entering the tube at time t achieve the same velocity $\bar{c}_{i,T}(t)$ and move together, forming a “plug”. Function $\bar{c}_{i,T}(t)$ is continuously differentiable.
2. Plugs may have different velocities but the velocity of a single plug stays constant during its travel along the tube.
3. Plugs cannot overtake each other (the First-In-First-Out or FIFO principle).

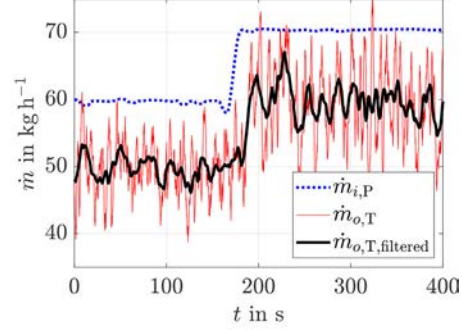
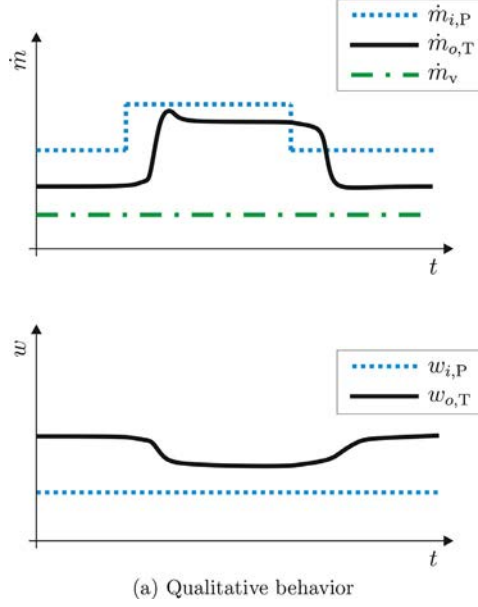


Fig. 3. I/o behavior of a single FFE pass

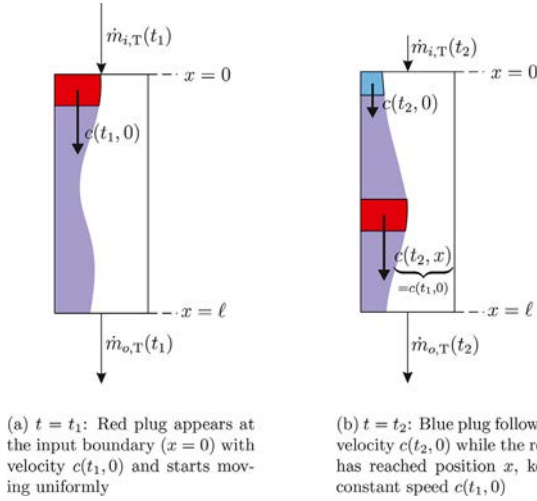


Fig. 4. Sketches of DPF

4. Plugs consist of separated, non-interacting parts: water and dry matter.
5. Infinitesimal vapor mass flow $\dot{\mu}_v(t, x) dx$ evaporates from the water part of the plug at point x and time t . Thus, $\dot{\mu}_v(t, x)$ is the linear density of the vapor mass flow distribution along the tube. The measurement unit of $\dot{\mu}_v$ is $\text{kg}/(\text{s} \cdot \text{m})$.

3.2. PDE Description of DPF

In order to obtain the partial differential equations of DPF, let us consider a tube of length ℓ and introduce the spatial variable x measured along the tube with $x = 0$ being the inlet and $x = \ell$ the outlet. State variables $\xi_w(t, x)$ and $\xi_d(t, x)$ will denote the linear density of water and dry content, respectively, over all n tubes of one pass (all tubes behave exactly similarly). Moreover, $c(t, x)$ denotes the flow velocity at a given point.

The PDEs are derived essentially in the same way that a simpler case is treated in (Winchester, 2000, pp. 26–31), i.e., by considering mass and momentum balances over infinitesimal flow ele-

ments. Thus, the following model is built, where $x \in [0, \ell]$, $t \geq t_0$:

$$\frac{\partial \xi_w(t, x)}{\partial t} + c(t, x) \frac{\partial \xi_w(t, x)}{\partial x} + \xi_w(t, x) \frac{\partial c(t, x)}{\partial x} = -\dot{\mu}_v(t, x), \quad (3a)$$

IC: $\xi_w(t_0, x) = \xi_{w,0}(x)$,

BC: $\xi_w(t, 0) = \frac{\dot{m}_{i,T}(t)(1 - w_{i,T}(t))}{c(t, 0)}$,

$$\frac{\partial \xi_d(t, x)}{\partial t} + c(t, x) \frac{\partial \xi_d(t, x)}{\partial x} + \xi_d(t, x) \frac{\partial c(t, x)}{\partial x} = 0, \quad (3b)$$

IC: $\xi_d(t_0, x) = \xi_{d,0}(x)$,

BC: $\xi_d(t, 0) = \frac{\dot{m}_{i,T}(t)w_{i,T}(t)}{c(t, 0)}$,

$$\frac{\partial c(t, x)}{\partial t} + c(t, x) \frac{\partial c(t, x)}{\partial x} = 0, \quad (3c)$$

IC: $c(t_0, x) = c_0(x)$,

BC: $c(t, 0) = \bar{c}_{i,T}(t)$,

Output 1: $\dot{m}_{o,T}(t) = (\xi_w(t, \ell) + \xi_d(t, \ell))c(t, \ell)$,

Output 2: $w_{o,T}(t) = \frac{\xi_d(t, \ell)}{\xi_w(t, \ell) + \xi_d(t, \ell)}$.

The mass balances for water and dry matter content yield (3a) and (3b). Equation (3c) is simply a mathematical formulation of Assumption 2 but it can also be interpreted as the momentum balance simplified by the assumption of one-dimensional flow and neglecting interaction between the plugs as well as external forces. The PDEs are equipped with initial conditions (IC), boundary conditions (BC, defined by the mass flow and dry mass content on the input boundary $x = 0$) and output values for mass flow and dry mass content taken at the output boundary $x = \ell$.

Observe that (3c) is the inviscid Burger's equation Polyanin and Zaitsev (2016); Sarra (2003). The solution of this equation may include singularities, so-called *shock waves*, that occur at the intersections of characteristics and must be treated as *generalized solutions*. We are not interested in studying shock waves because they can not appear in the real FFE due to the rather moderate and smooth nature of the falling film. Speaking about reality, the

liquid flow always exhibits some diffusion which can be modeled by adding the second-order term $D \frac{\partial^2 c(t,x)}{\partial x^2}$ to the right hand side of (3c). The diffusion inhibits formation of the shock waves, however, adding it would be a divergence from our original plan of focusing on first-order PDEs and would make it impossible to obtain a time-delay representation of the i/o dynamics. Therefore, we choose another way of avoiding the shock waves: to exclude them by enforcing a constraint on the rate of change of the input flow velocity. The constraint is specified below, see (6).

Our next goal is to convert the PDE model (3) to the time-delay form by solving it via the method of characteristics. Therefore, assumptions specifying the evaporation term $\dot{\mu}_v$ are necessary. In Sec. 3.3 and 3.4, we consider, respectively, uniform evaporation and evaporation proportional to the water content.

3.3. Input-Output Behavior of DPF with Uniform Evaporation Model

We recall the formula for the total vapor mass flow \dot{m}_v coming out of the tubes

$$\dot{m}_v(t) = \frac{k\pi d \ell n (\vartheta_H(t) - \vartheta_T(t))}{\Delta h_v(t)} \quad (4)$$

which follows from the energy balance Paramalingam (2004); Winchester (2000); Quaak et al. (1994). Generally, the heat transfer coefficient k in (4) depends on the dry matter content w of the liquid. However, including this feature would not let us solve the PDEs and obtain time-delay i/o equations of one FFE pass. Thus, in this model we use (4) with constant k identified for stationary input dry matter content $w_{i,T}$.

Remark 1. Dependence of the heat transfer coefficient k on dry matter content w is considered later in the model of overtaking particle flow (OPF) with localized evaporation, see Sec. 4.4.

The assumption of uniform evaporation along the tubes, i.e.,

$$\dot{\mu}_v(t, x) = q(t) \quad \text{with} \quad q(t) = \frac{\dot{m}_v(t)}{\ell} \quad (5)$$

is often applied in publications on modeling the dynamics of FFE tubes Winchester (2000); Paramalingam (2004); Quaak et al. (1994); Stefanov and Hoo (2003). Substituting (5) into (3a), we are ready to solve (3) and obtain the time-delay representation of the i/o dynamics.

Theorem 1 (Input-output behavior of DPF with uniform evaporation). Consider the DPF model given by (3), (5) and assume that the functions $\dot{m}_{i,T}(t) > 0$, $w_{i,T}(t) \in [0, 1]$, $\bar{c}_{i,T}(t) > 0$, $\xi_{w,0}(x) > 0$, $\xi_{d,0}(x) > 0$, $c_0(x) > 0$, and $\dot{m}_v(t) > 0$ are smooth and satisfy

$$\dot{\bar{c}}_{i,T}(t) < \frac{\bar{c}_{i,T}^2(t)}{\ell}, \quad \forall t \geq t_0, \quad (6)$$

$$\frac{dc_0(x)}{dx}(\ell - x) > -c_0(x), \quad \forall x \in [0, \ell], \quad (7)$$

$$c_0(0) = \bar{c}_{i,T}(t_0). \quad (8)$$

Then there exists the classical solution of the PDE system (3), (5). For

$$t \geq t_0 + \frac{\ell}{\bar{c}_{i,T}(t_0)} \quad (9)$$

the outputs $\dot{m}_{o,T}$ and $w_{o,T}$ are independent of the initial conditions and are solely determined by the boundary conditions (i.e., by the input variables $\dot{m}_{i,T}$, $w_{i,T}$ and $\bar{c}_{i,T}$). The i/o relations are then given by

the time-delay equations

$$\dot{m}_{o,T}(t) = \frac{\dot{m}_{i,T}(\theta)}{v(t, \theta)} \left(1 - \frac{\bar{c}_{i,T}(\theta)}{\dot{m}_{i,T}(\theta)} \int_{\theta}^t q(\alpha) v(\alpha, \theta) d\alpha \right) \Big|_{\theta=t-\tau(t)}, \quad (10a)$$

$$w_{o,T}(t) = w_{i,T}(\theta) \left(1 - \frac{\bar{c}_{i,T}(\theta)}{\dot{m}_{i,T}(\theta)} \int_{\theta}^t q(\alpha) v(\alpha, \theta) d\alpha \right)^{-1} \Big|_{\theta=t-\tau(t)} \quad (10b)$$

where the mass dispersion factor $v(\alpha, \theta)$ is defined as

$$v(\alpha, \theta) = 1 - \frac{\bar{c}_{i,T}(\theta)}{\dot{m}_{i,T}(\theta)} (\alpha - \theta) \quad (11)$$

and time delay $\tau(t)$ is implicitly defined by

$$\tau(t) = \frac{\ell}{\bar{c}_{i,T}(t - \tau(t))}. \quad (12)$$

Proof. The proof, shown in Appendix A, involves applying the method of characteristics to obtain the general solution of the PDEs (3) and consequently the outputs of the system. As explained in the Appendix, conditions (6)–(8) guarantee that the plugs cannot overtake one another, thus making sure that Assumption 3 is satisfied. \square

Remark 2. The problem of computing $\tau(t)$ according to (12) is addressed later in Sec. 3.5.

3.4. Input-Output Behavior of DPF with Water-Proportional Evaporation Model

Although the assumption of uniform evaporation is far-spread in the literature, it is prone to failure which becomes obvious if one considers a plug containing rather small amount of water. If evaporation is too active, such a plug may soon evaporate all its water content, i.e., ξ_w may become zero. Beyond that point, according to (3a), the variable ξ_w keeps decreasing and turns negative, in contradiction to its physical meaning.

The situation just described does not always take place: for instance, the uniform evaporation model works well in the simulations of Sec. 5 because there is “enough” water in the product, evaporation is “slow” and the product moves “quickly”, avoiding the drying out. Judging by its popularity, the uniform evaporation model probably works in most real scenarios happening in FFEs, however, it still is fragile.

To counter the problem, we introduce a more robust model where evaporation mass flow from a given plug is proportional to its water content, thus, the plug’s water content cannot go below zero. Instead, more vapor flow is redistributed to the plugs containing more water. This assumption allows the physical interpretation: water molecules jump from liquid to vapor with equal probability, i.e., where there is more water there is more evaporation.

Mathematically, the assumption is

$$\dot{\mu}_v(t, x) = b(t) \xi_w(t, x) \quad \text{with} \quad b(t) = \frac{\dot{m}_v(t)}{M_w(t)} \quad (13)$$

where the total vapor mass flow $\dot{m}_v(t)$ is given by (4) and M_w is the total mass of water inside the tubes:

$$M_w(t) = \int_0^\ell \xi_w(t, x) dx. \quad (14)$$

Factor $b(t)$ in (13) may be called *instantaneous evaporation rate*.

Theorem 2 (Input-output behavior of DPF with water-proportional evaporation). Consider the DPF model given by (3), (13) and assume that the functions $\dot{m}_{i,T}(t) > 0$, $w_{i,T}(t) \in [0, 1]$, $\bar{c}_{i,T}(t) > 0$, $\xi_{w,0}(x) > 0$, $\xi_{d,0}(x) > 0$, $c_0(x) > 0$, and $\dot{m}_v(t) > 0$ are smooth and satisfy (6), (7), (8). Then there exists the classical solution of the PDE system (3), (13). For

$$t \geq t_0 + \frac{\ell}{\bar{c}_{i,T}(t_0)} \quad (15)$$

the outputs $\dot{m}_{o,T}$ and $w_{o,T}$ are independent of the initial conditions and are solely determined by the boundary conditions (i.e., by the input variables $\dot{m}_{i,T}$, $w_{i,T}$ and $\bar{c}_{i,T}$). The i/o relations are then given by the time-delay equations

$$\dot{m}_{o,T}(t) = \frac{\dot{m}_{i,T}(\theta) [w_{i,T}(\theta) + (1 - w_{i,T}(\theta)) \beta(\theta, t)]}{v(t, \theta)} \Big|_{\theta=t-\tau(t)} \quad (16a)$$

$$w_{o,T}(t) = \frac{w_{i,T}(\theta)}{w_{i,T}(\theta) + (1 - w_{i,T}(\theta)) \beta(\theta, t)} \Big|_{\theta=t-\tau(t)} \quad (16b)$$

where notation (11), (12) is used and the integral evaporation rate $\beta(\theta, t)$ is defined as

$$\beta(\theta, t) = \exp \left(- \int_{\theta}^t b(\alpha) d\alpha \right). \quad (17)$$

The latter via the definition (13) of $b(t)$ depends on the total water mass $M_w(t)$ which is calculated for $t \geq t_0 + \ell/\bar{c}_{i,T}(t_0)$, as

$$M_w(t) = \int_{t-\tau(t)}^t \dot{m}_{i,T}(\theta) (1 - w_{i,T}(\theta)) \beta(\theta, t) d\theta. \quad (18)$$

Proof. Similarly to the proof of Theorem 1, the statement follows from the general solution of PDEs (3) under assumption (13) which is obtained in Appendix B. Observe that the time delay τ can be still defined via (12) because in our model evaporation does not affect the velocity of plugs. \square

Remark 3. Instead of (18), the overall mass of water M_w can be obtained via water mass balance over the tubes:

$$\frac{dM_w(t)}{dt} = (1 - w_{i,T}(t)) \dot{m}_{i,T}(t) - (1 - w_{o,T}(t)) \dot{m}_{o,T}(t) - \dot{m}_v(t). \quad (19)$$

However, this approach may lead to accumulation of the numerical integration error. Thus, the finite-time integration formula (18) is likely easier to implement numerically than (19).

3.5. Calculation of Time Delay

The time delay value $\tau(t)$ in the DPF model is expressed by the implicit equation (12). Using the definition directly during simulation is impractical. For this reason, we propose to resolve it using the method of dynamic inversion Getz and Marsden (1995). The method is to replace (12) with

$$\begin{aligned} & \frac{d}{dt} \left(\tau(t) \bar{c}_{i,T}(t - \tau(t)) - \ell \right) \\ & = -\gamma \left(\tau(t) \bar{c}_{i,T}(t - \tau(t)) - \ell \right), \quad \gamma = \text{const} > 0 \end{aligned} \quad (20)$$

where γ ensures exponentially decreasing equation error. Evaluating the derivative in (20) leads to the equation

$$\begin{aligned} \frac{d\tau(t)}{dt} & = \frac{\tau(t) \dot{\bar{c}}_{i,T}(\theta) + \gamma (\tau(t) \bar{c}_{i,T}(\theta) - \ell)}{\tau(t) \dot{\bar{c}}_{i,T}(\theta) - \dot{\bar{c}}_{i,T}(\theta)} \Big|_{\theta=t-\tau(t)}, \quad t \geq t_f, \\ \tau(t_f) & = t_f - t_0 \end{aligned} \quad (21)$$

where t_f is such that $t_f - \tau(t_f) = t_0$, so by (12)

$$t_f = t_0 + \frac{\ell}{\bar{c}_{i,T}(t_0)}. \quad (22)$$

Remark 4. In Cascetta (2013), the time-delay formulation (10) of the DPF is proposed for a general transportation system and is called *Dynamic Network Loading Model*. However, the relation to the corresponding PDE description and implementation of (12) are not discussed there. Moreover, neither sink nor source terms are considered in Cascetta (2013).

4. Second Transport Model: Overtaking Particle Flow (OPF)

4.1. General Principles of the Model

To enable overtaking of particles, we consider non-interacting particles moving in a two-dimensional space just like cars on a highway driving down parallel lanes (Fig. 5). Instead of a few lanes, however, we have a continuum: the ‘lanes’ are assigned specific velocities to them, ranging continuously from c_{\min} to c_{\max} . In other words, we extend the original spatial domain $[0, \ell]$ by adding the second coordinate $c \in [c_{\min}, c_{\max}]$. All particles having coordinate c move along the x axis with the same velocity c . As they are restricted to a separate lane, they can overtake neighboring particles on the slower lanes, hence the name OPF.

The input boundary $x = 0$ is populated with particles of the input mass flow according to some velocity distribution function. The distribution is generally time-varying. For instance, it is reasonable to suppose that the higher mass flow means predominantly faster particles which is represented by a distribution centered around a higher value of c . Accordingly, Fig. 5 shows the scenario when at time t_0 the input mass flow $\dot{m}_{i,T}(t_0)$ is small; its particles, colored blue, are assigned slower lanes, although some of them are a little faster than others. Later, at time t_1 , the blue particles have moved some distance towards the output; meanwhile, the input flow has increased and the new particles, colored red, are starting on the faster lanes. At time t_2 , the fast particles have overtaken the slow ones and arrive at the output first; they appear in the output mass flow.

To consider evaporation, the mass flow is split into two parallel flows: one for dry matter and another for water. Both flows gain the same velocities on the input boundary, the only difference being that water flow experiences evaporation.

4.2. PDE Description of OPF

Let us denote $\xi_w(t, x, c)$ and $\xi_d(t, x, c)$ the state of, respectively, water and dry matter flows. The value of $\xi_w(t, x, c)$ (and similarly $\xi_d(t, x, c)$ for dry matter) represents the areal density of water in the point (x, c) at time t . Areal density over the extended spatial domain $[0, \ell] \times [c_{\min}, c_{\max}]$ is understood as ‘mass divided by length and by velocity’. The dimensional unit of ξ_w and ξ_d is thus $\text{kg} \cdot \text{s}/\text{m}^2$.

To develop the PDE description of OPF with evaporation, we make the following assumptions:

1. Distribution of the input mass flow $\dot{m}_{i,T}(t)$ along the input boundary $x = 0$ is specified by time-varying ‘density’ function $f(c, t)$ satisfying

$$\int_{c_{\min}}^{c_{\max}} f(c, t) dc \equiv 1 \quad (23)$$

so that

$$\xi_w(t, 0, c) + \xi_d(t, 0, c) = f(c, t) \dot{m}_{i,T}(t) / c. \quad (24)$$

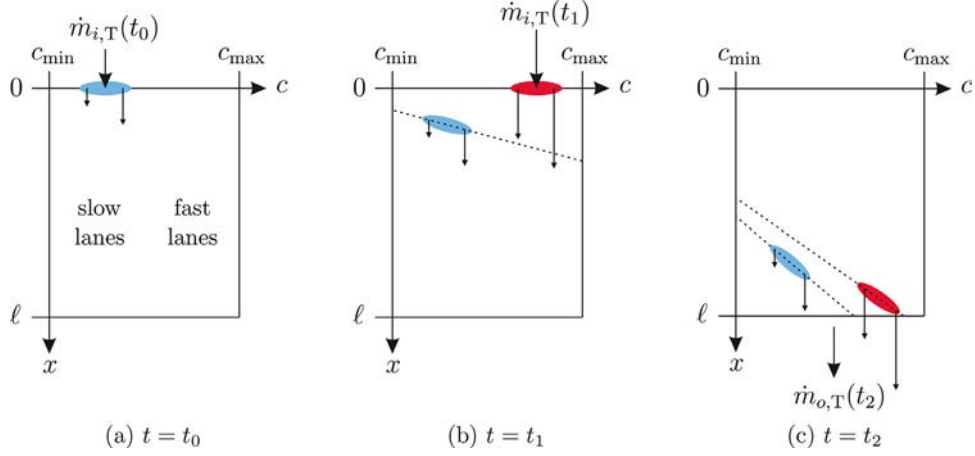


Fig. 5. Sketch of OPF

2. Water and dry matter particles follow the same velocity distribution which, together with the previous assumption, yields

$$\xi_w(t, 0, c) = f(t, c) \dot{m}_{i,T}(t) (1 - w_{i,T}(t)) / c. \quad (25a)$$

$$\xi_d(t, 0, c) = f(t, c) \dot{m}_{i,T}(t) w_{i,T}(t) / c. \quad (25b)$$

3. Velocity of each particle stays constant.

4. Infinitesimal evaporation mass flow in point x from the part of the water flow moving at velocity c is $\dot{\mu}_v(t, x, c) dx dc$. Therefore, $\dot{\mu}_v(t, x, c)$ is the areal density of the vapor mass flow distribution over the domain $[0, \ell] \times [c_{\min}, c_{\max}]$. The dimensional unit of $\dot{\mu}_v$ is kg/m^2 , i.e., mass flow divided by length and by velocity.

The mass balance yields the following PDEs, defined on $x \in [0, \ell]$, $t \geq t_0$, $c \in [c_{\min}, c_{\max}]$:

$$\frac{\partial \xi_w(t, x, c)}{\partial t} + c \frac{\partial \xi_w(t, x, c)}{\partial x} = -\dot{\mu}_v(t, x, c), \quad (26a)$$

$$\text{IC: } \xi_w(t_0, x, c) = \xi_{w,0}(x, c),$$

$$\text{BC: } \xi_w(t, 0, c) = f(c, t) \dot{m}_{i,T}(t) (1 - w_{i,T}(t)) / c,$$

$$\frac{\partial \xi_d(t, x, c)}{\partial t} + c \frac{\partial \xi_d(t, x, c)}{\partial x} = 0, \quad (26b)$$

$$\text{IC: } \xi_d(t_0, x, c) = \xi_{d,0}(x, c),$$

$$\text{BC: } \xi_d(t, 0, c) = f(c, t) \dot{m}_{i,T}(t) w_{i,T}(t) / c$$

$$\text{Output 1: } \dot{m}_{o,T}(t) = \int_{c_{\min}}^{c_{\max}} (\xi_w(t, \ell, c) + \xi_d(t, \ell, c)) c dc, \quad (26c)$$

$$\text{Output 2: } w_{o,T}(t) = \frac{1}{\dot{m}_{o,T}(t)} \int_{c_{\min}}^{c_{\max}} \xi_d(t, \ell, c) c dc. \quad (26d)$$

Remark 5. The velocity distribution function $f(c, t)$ is to be determined experimentally using parametric system identification techniques. Specifically, one can assume that $f(\cdot, t)$ belongs to a certain class of functions $[c_{\min}, c_{\max}] \rightarrow \mathbb{R}_{\geq 0}$ parameterized by a vector of time-varying parameters. The parameters may vary depending on the input mass flow, product concentration, etc. The choice of the class of distribution functions can be based on phenomenological

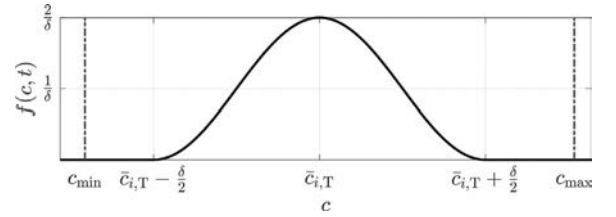


Fig. 6. Shape of the velocity distribution function (27)

or fundamental reasons. In this paper, for illustrative purposes, we use the cosine distribution (see Fig. 6):

$$f(c, t) = \begin{cases} \frac{1}{\delta} \left(1 + \cos \frac{2\pi(c - \bar{c}_{i,T}(t))}{\delta} \right), & |c - \bar{c}_{i,T}(t)| \leq \frac{\delta}{2}, \\ 0, & \text{otherwise} \end{cases} \quad (27)$$

where $\bar{c}_{i,T}(t)$ is the mean velocity which in our simulations depends on the input mass flow so that the larger the flow, the faster it is, see (1). The support of the distribution (27) is $\mathcal{C}(t) = [\bar{c}_{i,T}(t) - \delta/2, \bar{c}_{i,T}(t) + \delta/2]$. Thus, one must ensure that c_{\min} and c_{\max} are such that $\mathcal{C}(t) \subset [c_{\min}, c_{\max}]$ at all times, i.e., for all realistically possible values of $\bar{c}_{i,T}(t)$.

4.3. Input-Output Behavior of OPF with Water-Proportional Evaporation Model

The assumption of uniform evaporation which we regarded in the context of DPF (Sec. 3.3) is not suitable for OPF due to the fundamental reason that $\xi_w(t, x, c) = 0$ in some points (x, c) . Those points cannot evaporate any mass without ξ_w going negative which would not be physical. Thus, we skip the uniform evaporation and study evaporation proportional to the water content. It is defined similarly to (13), i.e.,

$$\dot{\mu}_v(t, x, c) = b(t) \xi_w(t, x, c) \quad \text{with} \quad b(t) := \frac{\dot{m}_v(t)}{M_w(t)}, \quad (28)$$

total vapor mass flow $\dot{m}_v(t)$ given by (4) and total mass of water calculated as

$$M_w(t) = \int_0^\ell \int_{c_{\min}}^{c_{\max}} \xi_w(t, x, c) dc dx. \quad (29)$$

Theorem 3 (Input-output behavior of OPF with water-proportional evaporation). *Consider the OPF model (26), (28) and assume that the functions $\dot{m}_{i,T}(t) > 0$, $w_{i,T}(t) \in [0, 1)$, $\bar{c}_{i,T}(t) > 0$, $\xi_{w,0}(x, c) > 0$,*

$\xi_{d,0}(x, c) > 0$, $\dot{m}_v(t) > 0$, and $f(c, t) > 0$ are smooth. Then there exists the classical solution of the PDE system (26), (28). For

$$t \geq t_0 + \frac{\ell}{c_{\min}} \quad (30)$$

the outputs $\dot{m}_{o,T}$ and $w_{o,T}$ are independent of the initial conditions and are solely determined by the boundary conditions (i.e., by the input variables $\dot{m}_{i,T}$, $w_{i,T}$ and input velocity distribution function f). The i/o relations are then given by the time-delay equations

$$\dot{m}_{o,T}(t) = \int_{c_{\min}}^{c_{\max}} f(c, \theta) \dot{m}_{i,T}(\theta) \left[w_{i,T}(\theta) + (1 - w_{i,T}(\theta)) \beta(\theta, t) \right] \Big|_{\theta=t-\ell/c} dc, \quad (31a)$$

$$w_{o,T}(t) = \frac{1}{\dot{m}_{o,T}(t)} \int_{c_{\min}}^{c_{\max}} f(c, \theta) \dot{m}_{i,T}(\theta) w_{i,T}(\theta) \Big|_{\theta=t-\ell/c} dc \quad (31b)$$

where notation (17) is used and the total water mass $M_w(t)$ is calculated as

$$M_w(t) = \int_0^\ell \int_{c_{\min}}^{c_{\max}} \frac{f(c, \theta) \dot{m}_{i,T}(\theta) (1 - w_{i,T}(\theta)) \beta(\theta, t)}{c} \Big|_{\theta=t-x/c} dc dx. \quad (32)$$

Proof. The i/o equations are obtained via the method of characteristics which gives the general solution of PDEs (26) under assumption (28), see Appendix C. \square

4.4. Input-Output Behavior of OPF with Localized Evaporation Model

In this subsection we introduce another evaporation model, namely, *localized evaporation*. Notice that the previously discussed uniform and water-proportional evaporation models are based on the calculation of the total vapor flow (4) from the whole tube and distribution thereof among the liquid flow elements (uniformly or proportionally to the water mass in a given element). The localized evaporation model, on the contrary, directly considers *local* evaporation from each flow element separately.

An advantage of the localized approach is that the local vapor mass flow can depend on the local properties of the product. It is indeed reasonable as the heat transfer coefficient k goes down as the dry matter fraction w increases which results in reduced evaporation Holman (1989).

Remark 6. Localized evaporation can in principle be applied to the DPF model as well. However, resulting PDEs are not solvable analytically. The difficulties arise essentially from the compressions and rarefactions in DPF due to varying plug velocities which complicates the dynamics of dry matter content $w(t, x)$. The problem can be avoided in OPF because the flow is split into separate “lanes” with different velocities (Fig. 5). Thus, we opt to study the localized evaporation model only in case of OPF.

The following assumptions specify the localized evaporation model under the requirement that the resulting PDEs be solvable explicitly and thus convertible to time-delay i/o relations:

1. To approximate the relationship between the heat transfer coefficient k and the dry mass fraction w , we adopt the linear model

$$k(w) = k_0 - k_1 w, \quad k_0, k_1 = \text{const} > 0 \quad (33)$$

proposed by Winchester Winchester (2000). Obviously, this model only makes sense for $w < k_0/k_1$. As dry mass fraction increases and approaches the limit value k_0/k_1 from below, k turns to zero and evaporation halts. Relation (33) applies to

each infinitesimal flow element, w then being the local dry mass fraction, i.e., the ratio $\xi_d/(\xi_w + \xi_d)$.

Linearity of (33) is crucial because it leads to a coupling between the PDEs for ξ_w and ξ_d in the form of a rational term which results in an integrable characteristic equation.

2. Let us call *siblings* the infinitesimal flow elements that originated on the input boundary $x=0$ at the same time, say t_1 , but with different c -coordinates. We will assume that the vapor flow from the siblings is distributed between them proportionally to the same distribution function $f(c, t_1)$ that was used to distribute the *input* flow among them.

This assumption simplifies the model by way of decoupling the dynamics of the group of siblings from the dynamics of other flow elements. Furthermore, it ensures that all siblings always have the same dry mass fraction, essentially decoupling them from each other.

Formalizing these ideas, vapor mass flow density in the point (x, c) is specified as

$$\dot{\mu}_v(t, x, c) = \phi(t, x, c) k(t, x, c) p(t) \quad (34)$$

where, in accordance with (33), the local heat transfer coefficient $k(t, x, c)$ is

$$k(t, x, c) = k_0 - k_1 \frac{\xi_d(t, x, c)}{\xi_w(t, x, c) + \xi_d(t, x, c)}, \quad (35)$$

the distribution factor $\phi(t, x, c)$, following the second assumption above, is governed by the equations

$$\begin{aligned} \frac{\partial \phi(t, x, c)}{\partial t} + c \frac{\partial \phi(t, x, c)}{\partial x} &= 0, \\ \text{IC: } \phi(0, x, c) &= \phi_0(x, c), \\ \text{BC: } \phi(t, 0, c) &= f(c, t) \end{aligned} \quad (36)$$

and the coefficient $p(t)$ is chosen to match (34) with the total vapor mass flow formula (4):

$$p(t) = \frac{\pi dn(\vartheta_H(t) - \vartheta_T(t))}{\Delta h_v(t)}. \quad (37)$$

Theorem 4 (Input-output behavior of OPF with localized evaporation). Consider the OPF model (26), (34)–(37) and assume that the functions $\dot{m}_{i,T}(t) > 0$, $w_{i,T}(t) \in [0, 1)$, $\bar{c}_{i,T}(t) > 0$, $\xi_{w,0}(x, c) > 0$, $\xi_{d,0}(x, c) > 0$, $\dot{m}_v(t) > 0$, and $f(c, t) > 0$ are smooth. Then there exists the classical solution of the PDE system (26), (34)–(37). For

$$t \geq t_0 + \frac{\ell}{c_{\min}} \quad (38)$$

the outputs $\dot{m}_{o,T}$ and $w_{o,T}$ are independent of the initial conditions and are solely determined by the boundary conditions (i.e., by the input variables $\dot{m}_{i,T}$, $w_{i,T}$ and input velocity distribution function f). The i/o relations are then given by the time-delay equations

$$\dot{m}_{o,T}(t) = \int_{c_{\min}}^{c_{\max}} f(c, \theta) \dot{m}_{i,T}(\theta) w_{i,T}(\theta) \Omega \left(\frac{1}{w_{i,T}(\theta)}, \frac{c \varpi(\theta, t)}{\bar{m}_{i,T}(\theta) w_{i,T}(\theta)} \right) \Big|_{\theta=t-\ell/c} dc, \quad (39a)$$

$$w_{o,T}(t) = \frac{1}{\dot{m}_{o,T}(t)} \int_{c_{\min}}^{c_{\max}} f(c, \theta) \dot{m}_{i,T}(\theta) w_{i,T}(\theta) \Big|_{\theta=t-\ell/c} dc \quad (39b)$$

where the function Ω is defined via the Lambert W -function as

$$\Omega(a, b) = \frac{k_1}{k_0} \left(W \left[\left(\frac{k_0}{k_1} a - 1 \right) \exp \left(\frac{k_0}{k_1} a - 1 - \frac{k_0^2}{k_1} b \right) \right] + 1 \right) \quad (40)$$

and we use the abbreviation

$$\varpi(\theta, t) = \int_{\theta}^t p(\alpha) d\alpha. \quad (41)$$

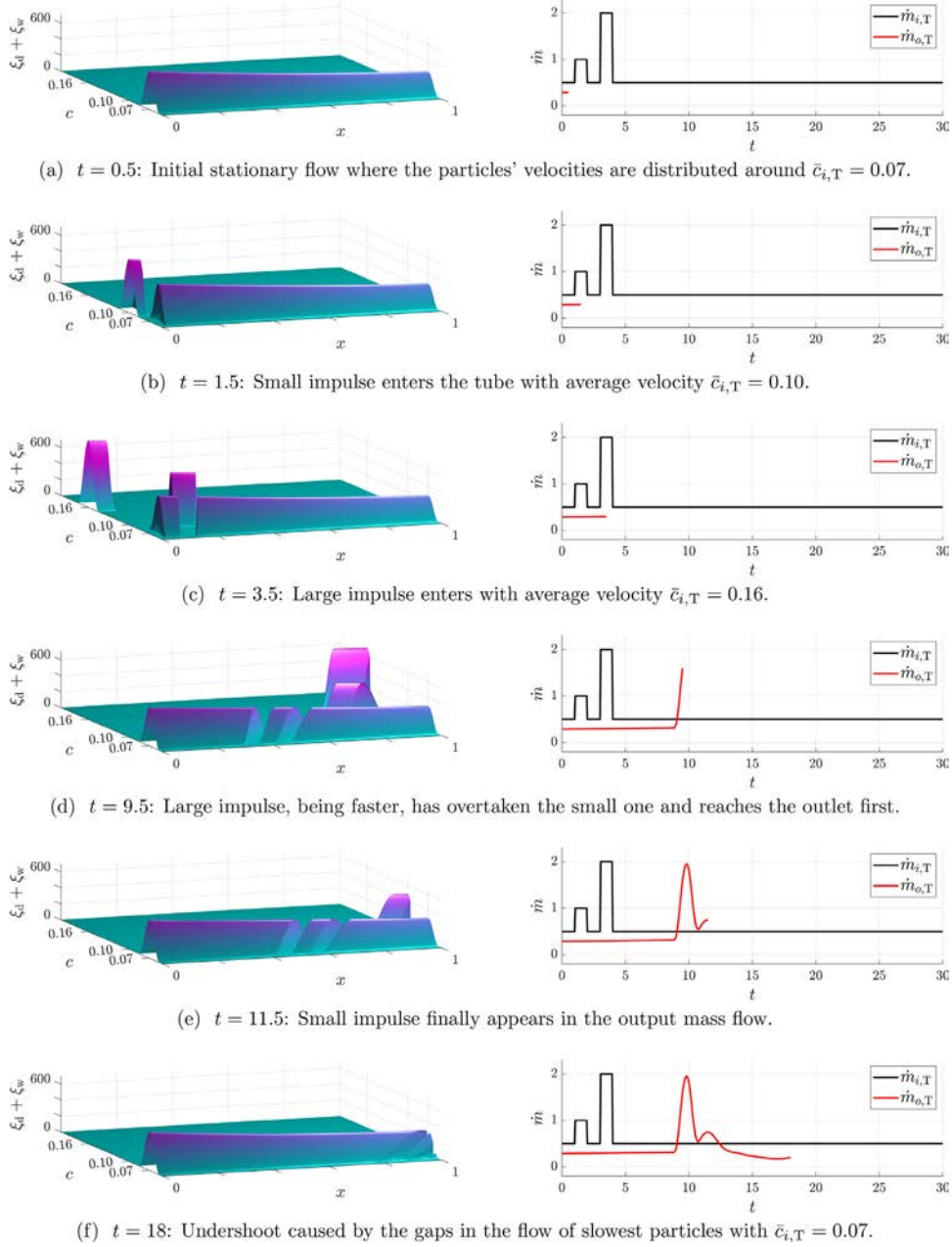


Fig. 7. Still frames from the animation of the illustrative OPF example

Proof. The i/o equations are obtained via the method of characteristics which gives the general solution of the PDE system (26) with (34)–(37), see Appendix D. \square

4.5. Animation of Illustrative Example

In order to visualize the behavior of the OPF model with water-proportional evaporation, let us consider an example. The animation of the combined “water + dry matter” PDE state $\xi_d + \xi_w$ as well as the mass flows $\dot{m}_{i,T}$ and $\dot{m}_{o,T}$ can be found online as Supplementary Material for this paper. Figure 7 shows several snapshots from the video.

The animation corresponds to the following scenario. Initially, the flow is stationary with input mass flow $\dot{m}_{i,T} = 0.5$ and constant vapor mass flow $\dot{m}_v \equiv 0.2$. Some time later, two impulses appear in

the input mass flow, a small one followed by a larger one, so that

$$\dot{m}_{i,T}(t) = \begin{cases} 1, & 1 \leq t \leq 2, \\ 2, & 3 \leq t \leq 4, \\ 0.5, & \text{otherwise.} \end{cases}$$

The average flow velocity depends on the mass flow according to the formula

$$\bar{c}_{i,T}(t) = 0.04 + 0.06 \dot{m}_{i,T}(t)$$

and the velocity distribution function is chosen to be cosine (27) with $\delta = 0.02$. The dry mass fraction of the incoming liquid is $w_{i,T}(t) \equiv 0.36$ and the length of the tube is $\ell = 1$.

Let us point out a few features in Fig. 7:

1. Overtaking of the small and slow mass flow impulse by the large and fast one is apparent between Fig. 7 and 7.
2. As the impulses are faster than the “normal” mass flow of 0.5, they take up positions with larger c -values and leave gaps in

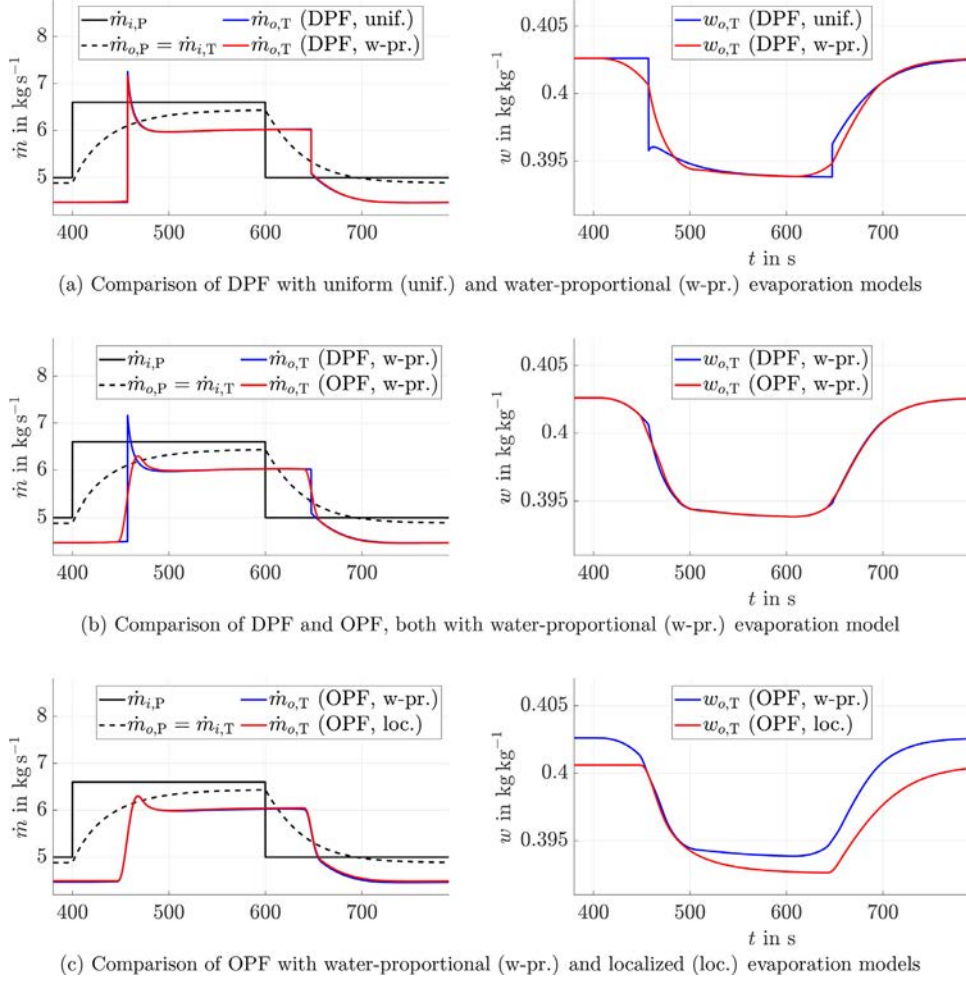


Fig. 8. Simulations of DPF and OPF with different evaporation models

the area of small c . The gaps, when they arrive at the output boundary, appear as an undershoot in the output mass flow (Fig.). The undershoot is apparent in the output because the input steps are sharp. Compare it to the more realistic scenario in Fig. 8c below where the input mass flow is filtered by the distribution plate and no undershoot is observed.

- Water-proportional evaporation leads to an exponential shape of the stationary state function ξ_w which can be observed in Fig. 7.

5. Simulation

In this section, the simulation results of the novel DPF and OPF models of Sec. 3 and 4 are compared to the qualitative i/o behavior in Fig. 3.

To simulate realistic situations, up/down-steps of the mass flow into the plate are executed between the levels $\dot{m}_{i,P0}$ and $\dot{m}_{i,P1}$. These scenarios occur during ramp-up of the falling film evaporator or when changing the operation point Schwaer et al. (2020). The parameters and constants used for this study are shown in Table 2 and refer to the first of four passes in an FFE used in the process of milk powder production. Time-varying liquid properties of the milk, such as density ρ and dynamic viscosity η , are calculated using the correlations in Schwaer et al. (2020). Simulations of this study include the distribution plate dynamics from Schwaer et al. (2020).

Table 2

Parameters and constants for the simulation-based model comparison.

Symbol	Value	Unit
A_0	0.005	m^2
A_p	2.14	m^2
c_{\max}	0.44	m s^{-1}
c_{\min}	0.22	m s^{-1}
d	0.05	m
g	9.81	m s^{-2}
k	1045	$\text{W m}^{-2} \text{K}^{-1}$
k_0	1896	$\text{W m}^{-2} \text{K}^{-1}$
k_1	2361	$\text{W m}^{-2} \text{K}^{-1}$
ℓ	17.7	m
n	131	-
$\dot{m}_{i,P0}$	5	kg s^{-1}
$\dot{m}_{i,P1}$	6.6	kg s^{-1}
$w_{i,P}$	0.36	kg kg^{-1}
γ	10	s^{-1}
δ	0.15	m s^{-1}
ϑ_H	57.3	$^\circ\text{C}$
$\vartheta_{i,P}$	72	$^\circ\text{C}$
ϑ_T	54.7	$^\circ\text{C}$

Falling film dynamics are implemented in Simulink in the form of time-delay i/o equations:

- (10), (21) for DPF with uniform evaporation;
- (16), (18), (21) for DPF with water-proportional evaporation;

- (31), (32) for OPF with water-proportional evaporation.
- (39) for OPF with localized evaporation.

All models assume the same average input velocity function (1): the larger the flow, the higher its velocity. For OPF, the cosine velocity distribution function (27) is used. The integral delays in the models are approximated with finite sums where the number of summands is selected empirically taking into account how fast the processes are. The model has the structure of a finite-time integrator and thus the numerical error caused by the approximation is not accumulated.

The time delay blocks in Simulink are initialized with arbitrary but realistic values. After 400 seconds of simulation time, when the stationary flow has established, the up/down-steps in $\dot{m}_{i,P}$ are performed.

Remark 7. Alternatively to the time-delay equations, PDE models (3) and (26) could be implemented in Simulink directly with the method developed in Ponomarev et al. (2020).

Figure 8 depicts comparative simulation results. Let us make some observations:

1. All models respond to an up-step in the input mass flow with an overshoot. It qualitatively agrees with the expected behavior (Fig. 3).
2. Water-proportional evaporation model, both for DPF and OPF, causes immediate response to a change in $\dot{m}_{i,T}$, particularly in terms of $w_{o,T}$ (Fig. 8). Indeed, an increase in the amount of incoming water immediately increases evaporation mass flow near the inlet and decreases it near the outlet; as a result, the output dry matter content starts going down. The symmetric effect is present when input mass flow decreases.
3. Uniform and localized evaporation models, on the other hand, exhibit a distinct delay followed by a transient, both in the output mass flow and output dry matter content (Figs. 8, 8 c).
4. OPF exhibits smoother transients in $\dot{m}_{o,T}$ compared to DPF (Fig. 8). It is explained by the diffusion-like properties of the velocity distribution function inside OPF.
5. Switching DPF to OPF while using the same water-proportional evaporation model affects $\dot{m}_{o,T}$ more noticeably than $w_{o,T}$ (Fig. 8). Conversely, changing the evaporation model has more effect on $w_{o,T}$ than on $\dot{m}_{o,T}$ (Figs. 8, 8 c).
6. The lower $w_{o,T}$ of OPF with localized evaporation compared to the other models (Fig. 8c) is explained by the dependence (33) of the heat transfer coefficient on the local dry matter content: as the latter goes up, the former decreases, resulting in reduced local evaporation.

6. Conclusion and Outlook

In pursuit of a control-oriented model of the falling film evaporator two new transport models to describe the falling film have been developed: Dynamic Plug Flow (DPF) and Overtaking Particle Flow (OPF). Furthermore, in addition to the well-known uniform evaporation model two new ones have been proposed, motivated by technical as well as fundamental reasons: water-proportional and localized evaporation. The models are expressed as systems of hyperbolic partial differential equations and as input-output time-delay equations. The latter are advantageous from the simulation viewpoint.

Comparative simulations provide some insight into choosing the transport and evaporation models. The choice between the transport models (DPF vs. OPF) can be made knowing that OPF produces smoother output mass flow compared to DPF due to a diffusion-like effect. However, the amount of calculation associated with simulation of OPF is higher because of its distributed integral delay as opposed to the pointwise delay in DPF.

If DPF is selected, there are two alternatives for the evaporation model: uniform and water-proportional. The latter yields smoother transient in the output dry matter content. Another difference that should be taken into account: uniform evaporation model exhibits delayed initial response whereas the water-proportional one responds immediately to any changes in the input mass flow. Arguably, the instant response at the output is unrealistic. However, the *main* part of the transient is still delayed. Therefore, depending on whether the instant response is small enough to be regarded as a modeling error, the water-proportional evaporation model may still prove useful.

If, on the other hand, OPF is the favored transport model, then the choice of evaporation model is between water-proportional and localized. Unlike water-proportional model which again responds instantly to any changes in the input mass flow, localized evaporation demonstrates a purely delayed transient. Water-proportional model is more computationally expensive due to the need of calculating the total mass of water inside the tube in the form of a double integral. Localized evaporation model, although simpler numerically, contains an important part that may require nontrivial experimental identification, namely, the heat transfer coefficient as a function of the dry matter content.

In the upcoming paper Hofmann et al., (2021) we demonstrate the results of experimental identification and validation of the OPF model with water-proportional evaporation. The experiments have been done at a pilot plant representing one tube of the FFE. They show that the model is a good description of the real process. Prospective work includes integration of this falling film model into the full multi-pass evaporator model. The complete model can be used for numerical experiments, operator training and other purposes. In the next step, it may require further simplification to enable system-theoretic control design process. The end goal is a “new and improved” multivariable control system.

Declaration of Competing Interest

The authors have no affiliation with any organization with a direct or indirect financial interest in the subject matter discussed in the manuscript.

Acknowledgments

The authors thank GEA Wiegand GmbH for technical information regarding the falling film evaporator process. Additionally, the authors thank the Initiative and Networking Fund of the Helmholtz Association in the future topic Energy Systems Integration”.

Appendix A. Proof of Theorem 1

Here we prove Theorem 1 which asserts the input-output relations for the DPF model with uniform evaporation. Initially, in the following Lemma we derive the solution of the DPF equations (3) under the uniform evaporation assumption (5) using the standard method of characteristics Courant and Hilbert (1989). Afterwards, the input-output relations are obtained from the PDE solution, proving the Theorem.

Lemma 1. *Under the conditions of Theorem 1 the PDE system (3), (5) admits the classical solution given, for $t \in [t_0, t_0 + \ell/c_0(0)]$, by*

$$\xi_w(t, x) = \frac{1}{\mu(t, x)} \left(\xi_{w,0}(x_i(t, x)) - \int_{t_0}^t q(\alpha) \mu(\alpha, x) d\alpha \right), \quad (\text{A.1a})$$

$$\xi_d(t, x) = \frac{\xi_{d,0}(x_i(t, x))}{\mu(t, x)}, \quad (\text{A.1b})$$

$$c(t, x) = c_0(x_i(t, x)), \quad (\text{A.1c})$$

$$x_i(t, x) = x - c_0(x_i(t, x))(t - t_0) \quad (\text{A.1d})$$

where

$$\mu(t, x) := 1 + \frac{dc_0(x)}{dx} \Big|_{x_i(t, x)} (t - t_0) \quad (\text{A.2})$$

and, for $t \geq t_0 + \ell/\bar{c}_{i,T}(t_0)$, by

$$\xi_w(t, x) = \frac{1}{v(t, \theta)} \left(\frac{\dot{m}_{i,T}(\theta) (1 - w_{i,T}(\theta))}{\bar{c}_{i,T}(\theta)} - \int_{\theta}^t q(\alpha) v(\alpha, \theta) d\alpha \right) \Big|_{\theta=t_i(t, x)}, \quad (\text{A.3a})$$

$$\xi_d(t, x) = \frac{\dot{m}_{i,T}(\theta) w_{i,T}(\theta)}{v(t, \theta) \bar{c}_{i,T}(\theta)} \Big|_{\theta=t_i(t, x)}, \quad (\text{A.3b})$$

$$c(t, x) = \bar{c}_{i,T}(t_i(t, x)), \quad (\text{A.3c})$$

$$t_i(t, x) = t - \frac{x}{\bar{c}_{i,T}(t_i(t, x))} \quad (\text{A.3d})$$

where

$$v(t, \theta) := 1 - \frac{\dot{\bar{c}}_{i,T}(\theta)}{\bar{c}_{i,T}(\theta)} (t - \theta). \quad (\text{A.4})$$

Proof. Direct application of the method of characteristics to (3) is not possible due to the terms $\xi_w \frac{\partial c}{\partial x}$ in (3a) and $\xi_d \frac{\partial c}{\partial x}$ in (3b). However, by introducing the variable $\zeta(t, x) := \frac{\partial c(t, x)}{\partial x}$, the system (3) of three PDEs with assumption (5) can be transformed into the following system of four PDEs

$$\frac{\partial \xi_w(t, x)}{\partial t} + c(t, x) \frac{\partial \xi_w(t, x)}{\partial x} = -\xi_w(t, x) \zeta(t, x) - q(t), \quad (\text{A.5a})$$

$$\text{IC: } \xi_w(t_0, x) = \xi_{w,0}(x),$$

$$\text{BC: } \xi_w(t, 0) = \frac{\dot{m}_{i,T}(t) (1 - w_{i,T}(t))}{c(t, 0)},$$

$$\frac{\partial \xi_d(t, x)}{\partial t} + c(t, x) \frac{\partial \xi_d(t, x)}{\partial x} = -\xi_d(t, x) \zeta(t, x), \quad (\text{A.5b})$$

$$\text{IC: } \xi_d(t_0, x) = \xi_{d,0}(x),$$

$$\text{BC: } \xi_d(t, 0) = \frac{\dot{m}_{i,T}(t) w_{i,T}(t)}{c(t, 0)},$$

$$\frac{\partial c(t, x)}{\partial t} + c(t, x) \frac{\partial c(t, x)}{\partial x} = 0, \quad (\text{A.5c})$$

$$\text{IC: } c(t_0, x) = c_0(x),$$

$$\text{BC: } c(t, 0) = \bar{c}_{i,T}(t),$$

$$\frac{\partial \zeta(t, x)}{\partial t} + c(t, x) \frac{\partial \zeta(t, x)}{\partial x} = -\zeta^2(t, x), \quad (\text{A.5d})$$

$$\text{IC: } \zeta(t_0, x) = \frac{dc_0(x)}{dx},$$

$$\text{BC: } \zeta(t, 0) = -\frac{\dot{\bar{c}}_{i,T}(t)}{\bar{c}_{i,T}(t)} \quad \text{with} \quad \dot{\bar{c}}_{i,T}(t) := \frac{d}{dt} \bar{c}_{i,T}(t),$$

$$\text{Output 1: } \dot{m}_{o,T}(t) = (\xi_w(t, \ell) + \xi_d(t, \ell))c(t, \ell),$$

$$\text{Output 2: } w_{o,T}(t) = \frac{\xi_d(t, \ell)}{\xi_w(t, \ell) + \xi_d(t, \ell)}.$$

Let us introduce the parameterization $(\tilde{t}(\sigma), \tilde{x}(\sigma))$, $\sigma \geq 0$, of the characteristic time-space curves and denote the values of the dependent variables on the curves using the abbreviation

$$\tilde{\square}(\sigma) := \square(\tilde{t}(\sigma), \tilde{x}(\sigma)) \quad (\text{A.6})$$

where \square is one of the functions ξ_w , ξ_d , c or ζ . Comparing the coefficients of the identity

$$\frac{d\tilde{t}}{d\sigma} \frac{\partial \tilde{\square}}{\partial \tilde{t}} + \frac{d\tilde{x}}{d\sigma} \frac{\partial \tilde{\square}}{\partial \tilde{x}} = \frac{d\tilde{\square}}{d\sigma} \quad (\text{A.7})$$

to the PDEs (A.5) with (5), the system of characteristic equations is obtained:

$$\frac{d\tilde{t}(\sigma)}{d\sigma} = 1, \quad (\text{A.8a})$$

$$\frac{d\tilde{x}(\sigma)}{d\sigma} = \tilde{c}(\sigma), \quad (\text{A.8b})$$

$$\frac{d\tilde{\xi}_w(\sigma)}{d\sigma} = -\tilde{\xi}_w(\sigma) \tilde{\zeta}(\sigma) - q(\tilde{t}(\sigma)), \quad (\text{A.8c})$$

$$\frac{d\tilde{\xi}_d(\sigma)}{d\sigma} = -\tilde{\xi}_d(\sigma) \tilde{\zeta}(\sigma), \quad (\text{A.8d})$$

$$\frac{d\tilde{c}(\sigma)}{d\sigma} = 0, \quad (\text{A.8e})$$

$$\frac{d\tilde{\zeta}(\sigma)}{d\sigma} = -\tilde{\zeta}^2(\sigma). \quad (\text{A.8f})$$

The solution of the ODEs (A.8) is

$$\tilde{t}(\sigma) = \tilde{t}(0) + \sigma, \quad (\text{A.9a})$$

$$\tilde{x}(\sigma) = \tilde{x}(0) + \tilde{c}(0)\sigma, \quad (\text{A.9b})$$

$$\tilde{\xi}_w(\sigma) = \frac{1}{1 + \tilde{\zeta}(0)\sigma} \left(\tilde{\xi}_w(0) - \int_0^\sigma q(\tilde{t}(0) + \alpha) (1 + \tilde{\zeta}(0)\alpha) d\alpha \right), \quad (\text{A.9c})$$

$$\tilde{\xi}_d(\sigma) = \frac{\tilde{\xi}_d(0)}{1 + \tilde{\zeta}(0)\sigma}, \quad (\text{A.9d})$$

$$\tilde{c}(\sigma) = \tilde{c}(0), \quad (\text{A.9e})$$

$$\tilde{\zeta}(\sigma) = \frac{\tilde{\zeta}(0)}{1 + \tilde{\zeta}(0)\sigma}. \quad (\text{A.9f})$$

Looking to find the solution of the PDEs (A.5) in a given point (t, x) , we are interested in the characteristic curve $(\tilde{t}(\cdot), \tilde{x}(\cdot))$ that passes through the point (t, x) , i.e., the curve that satisfies the boundary condition

$$\tilde{t}(\sigma) = t, \quad \tilde{x}(\sigma) = x \quad (\text{A.10})$$

with some $\sigma > 0$. As for the other boundary condition, let us pick the point $(\tilde{t}(0), \tilde{x}(0))$. Recall that, in terms of plug flow, the characteristic curve $(\tilde{t}(\cdot), \tilde{x}(\cdot))$ is the trajectory of a single plug, so $(\tilde{t}(0), \tilde{x}(0))$ determines the time and place of "birth" of the plug. There are two possibilities regarding the plug's origin:

1. Suppose the plug crossing the point x at time t originated from the initial mass distribution. Let the initial (at $t = t_0$) position of that plug be denoted $x_i(t, x) \in [0, \ell]$, then the corresponding characteristic satisfies the boundary condition

$$\tilde{t}(0) = t_0, \quad \tilde{x}(0) = x_i(t, x). \quad (\text{A.11})$$

Substituting (A.10) and (A.11) into (A.9), unwrapping the notation (A.6) and using the initial conditions from the PDEs (A.5), we get (A.1). The conclusion is valid for t such that $x_i(t, x) \geq 0$ which is simplified by the following consideration:

$$(A.1d) \Rightarrow \begin{cases} \frac{\partial x_i(t, x)}{\partial t} = - \frac{dc_0(x)}{dx} \Big|_{x_i(t, x)} \frac{\partial x_i(t, x)}{\partial t} (t - t_0) - c_0(x_i(t, x)), \\ t - t_0 = \frac{x - x_i(t, x)}{c_0(x_i(t, x))} \end{cases} \quad (\text{A.12a})$$

$$\Rightarrow \frac{\partial x_i(t, x)}{\partial t} = \frac{c_0^2(x_i(t, x))}{\frac{dc_0(x)}{dx} \Big|_{x_i(t, x)} (x - x_i(t, x)) + c_0(x_i(t, x))} \quad (\text{A.12b})$$

$$\stackrel{(7)}{\Rightarrow} \left[x_i(t, x) \in [0, x] \subset [0, \ell] \Rightarrow \frac{\partial x_i(t, x)}{\partial t} < 0 \right] \quad (\text{A.12c})$$

and since, by (A.1d), $x_i(t_0, x) = x$ and $x_i(t_1, x) = 0$ for $t_1 = t_0 + x/c_0(0)$, we conclude that $x_i(t, x) \geq 0$ for $t \in [t_0, t_1]$ as a strictly decreasing function on the interval. Hence, (A.1) is indeed valid for all $t \in [t_0, t_1]$, as reflected in the statement of the Lemma.

2. Suppose the plug crossing the point x at time t originated from the input mass flow. Let $t_i(t, x) \geq t_0$ be the moment that the plug enters through the input boundary $x = 0$. Then the boundary condition for the corresponding characteristic is

$$\tilde{t}(0) = t_i(t, x), \quad \tilde{x}(0) = 0. \quad (\text{A.13})$$

Similarly to the previous case, we obtain the expression (A.3) which applies for t such that $t_i(t, x) \geq t_0$. Then we find

$$(A.3d) \Rightarrow \frac{\partial t_i(t, x)}{\partial t} = 1 + \frac{x \tilde{c}_{i,T}(t_i(t, x))}{\tilde{c}_{i,T}^2(t_i(t, x))} \frac{\partial t_i(t, x)}{\partial t} \quad (\text{A.14a})$$

$$\Rightarrow \frac{\partial t_i(t, x)}{\partial t} = \frac{\tilde{c}_{i,T}^2(t_i(t, x))/x}{\tilde{c}_{i,T}^2(t_i(t, x))/x - \tilde{c}_{i,T}(t_i(t, x))} \quad (\text{A.14b})$$

$$\stackrel{(6)}{\Rightarrow} \left[t_i(t, x) \geq t_0 \Rightarrow \frac{\partial t_i(t, x)}{\partial t} > 0 \right] \quad (\text{A.14c})$$

and since, by (A.3d), $t_i(t_1, x) = t_0$ for $t_1 = t_0 + x/\tilde{c}_{i,T}(t_0)$, we conclude that $t_i(t, x) \geq t_0$ for $t \geq t_1$ as a strictly increasing function on the interval. Hence, (A.3) is indeed valid for all $t \geq t_1$, as reflected in the statement of the Lemma.

According to (8), which asserts $c_0(0) = \tilde{c}_{i,T}(t_0)$, the two cases just considered cover all $t \geq t_0$ without overlap. Thus, the solution is complete and single-valued.

The velocity constraints (6) and (7) ensure that the denominators of the expressions appearing in the Lemma, i.e., $\mu(t, x)$ and $\nu(t, x)$, are strictly positive. Thus, the solution is continuous.

Let us finally prove that there is no overtaking between the plugs. Firstly, consider the plugs from the initial distribution and recall that $x_i(t, x)$ is defined as the starting position of such a plug that at time t crosses the point x . It follows from (A.12c) that the further the plug starts from the point x , the later it will appear there. Similarly, take a plug from the input flow. From (A.14c), the later the plug enters the tube, the later it reaches the point x . Furthermore, the plugs from the initial distribution and those from the input flow do not cross paths because, due to (8), the "initial" plug starting at the inlet ($x = 0$) and the "input" plug entering first

(at $t = t_0$) move with the same velocity. Thus, there is no overtaking, and the solution is classical. \square

Remark 8. The values μ and ν in Lemma 1 may be called *mass dispersion factors* as they are responsible for the gradual changes in the linear density profile due to the velocity differences of the neighboring plugs.

To finalize the proof of Theorem 1, it remains to substitute $x = \ell$ in (A.3) which yields, for $t \geq t_0 + \ell/\tilde{c}_{i,T}(t_0)$,

$$\dot{m}_{o,T}(t) = \frac{\dot{m}_{i,T}(\theta)}{\nu(t, \theta)} \left(1 - \frac{\tilde{c}_{i,T}(\theta)}{\dot{m}_{i,T}(\theta)} \int_{\theta}^t q(\alpha) \nu(\alpha, \theta) d\alpha \right) \Big|_{\theta=t_i(t, \ell)}, \quad (\text{A.15a})$$

$$w_{o,T}(t) = w_{i,T}(\theta) \left(1 - \frac{\tilde{c}_{i,T}(\theta)}{\dot{m}_{i,T}(\theta)} \int_{\theta}^t q(\alpha) \nu(\alpha, \theta) d\alpha \right) \Big|_{\theta=t_i(t, \ell)}^{-1} \quad (\text{A.15b})$$

whence, employing the time delay $\tau(t)$ introduced by the formula $\tau(t) := t - t_i(t, \ell)$,

$$(\text{A.16})$$

the statement of Theorem 1 is reached.

Appendix B. Proof of Theorem 2

Here we outline the proof of Theorem 2 describing the input-output relations for the DPF with water-proportional evaporation. The following Lemma states the solution of the DPF equations (3) under evaporation proportional to the water content (13). Thereafter, the input-output equations are obtained.

Lemma 2. Under the conditions of Theorem 2 the PDE system (3), (13) admits the classical solution given, for $t \in [t_0, t_0 + \ell/c_0(0)]$, by

$$\xi_w(t, x) = \frac{\xi_{w,0}(x_i(t, x)) \beta(t_0, t)}{\mu(t, x)}, \quad (\text{B.1a})$$

$$\xi_d(t, x) = \frac{\xi_{d,0}(x_i(t, x))}{\mu(t, x)}, \quad (\text{B.1b})$$

$$c(t, x) = c_0(x_i(t, x)), \quad (\text{B.1c})$$

$$x_i(t, x) = x - c_0(x_i(t, x))(t - t_0) \quad (\text{B.1d})$$

where

$$\beta(t_1, t_2) := \exp \left(- \int_{t_1}^{t_2} b(\alpha) d\alpha \right) \quad (\text{B.2})$$

and, for $t \geq t_0 + \ell/\tilde{c}_{i,T}(t_0)$, by

$$\xi_w(t, x) = \frac{\dot{m}_{i,T}(\theta) (1 - w_{i,T}(\theta)) \beta(\theta, t)}{\nu(t, \theta) \tilde{c}_{i,T}(\theta)} \Big|_{\theta=t_i(t, x)}, \quad (\text{B.3a})$$

$$\xi_d(t, x) = \frac{\dot{m}_{i,T}(\theta) w_{i,T}(\theta)}{\nu(t, \theta) \tilde{c}_{i,T}(\theta)} \Big|_{\theta=t_i(t, x)}, \quad (\text{B.3b})$$

$$c(t, x) = \tilde{c}_{i,T}(t_i(t, x)), \quad (\text{B.3c})$$

$$t_i(t, x) = t - \frac{x}{\tilde{c}_{i,T}(t_i(t, x))}. \quad (\text{B.3d})$$

The factors $\mu(t, x)$ and $\nu(t, x)$ are defined by (A.2) and (A.4).

Proof. The PDEs are solved similarly to the case of uniform evaporation (Appendix A). The only difference is in the behavior of ξ_w . The corresponding characteristic equation becomes

$$\frac{d\tilde{\xi}_w(\sigma)}{d\sigma} = -\tilde{\xi}_w(\sigma)(b(\tilde{t}(\sigma)) + \tilde{\zeta}(\sigma)) \quad (\text{B.4})$$

and the general solution thereof is

$$\tilde{\xi}_w(\sigma) = \frac{\tilde{\xi}_w(0) \beta(\tilde{t}(0), \tilde{t}(0) + \sigma)}{1 + \tilde{\zeta}(0)\sigma}. \quad (\text{B.5})$$

The rest of the proof repeats that of Lemma 1. \square

To arrive at the equations (16) of Theorem 2, we substitute $x = \ell$ in (B.3) and introduce the time delay again as $\tau(t) := t - t_1(t, \ell)$. This yields the outputs of the model (3), (13) for $t \geq t_0 + \ell/\tilde{c}_{i,T}(t_0)$ in the desired form (16). As we note that equations (16) implicitly (via β) involve the total water mass $M_w(t)$, the latter is calculated for $t \geq t_0 + \ell/\tilde{c}_{i,T}(t_0)$ by plugging (B.3a) in (14) and obtaining (18).

Appendix C. Proof of Theorem 2

Here we prove Theorem 3 which gives the input-output relations for the OPF model with water-proportional evaporation. In the following Lemma we derive the solution of the OPF equations (26) under the water-proportional evaporation assumption (28). Then, the input-output relations are obtained from the PDE solution, proving the Theorem.

Lemma 3. Under the conditions of Theorem 3 the PDE system (26), (28) admits the classical solution given, for $t \in [t_0, t_0 + x/c]$, by

$$\xi_w(t, x, c) = \xi_{w,0}(x - (t - t_0)c, c) \beta(t_0, t), \quad (\text{C.1a})$$

$$\xi_d(t, x, c) = \xi_{d,0}(x - (t - t_0)c, c) \quad (\text{C.1b})$$

and, for $t \geq t_0 + x/c$, by

$$\xi_w(t, x, c) = f(c, \theta) \dot{m}_{i,T}(\theta) (1 - w_{i,T}(\theta)) \beta(\theta, t) / c \Big|_{\theta=t-x/c}, \quad (\text{C.2a})$$

$$\xi_d(t, x, c) = f(c, \theta) \dot{m}_{i,T}(\theta) w_{i,T}(\theta) / c \Big|_{\theta=t-x/c}. \quad (\text{C.2b})$$

Proof. As (26) is a system of 2-dimensional (in space) PDEs, the characteristic curve is defined in the 3-dimensional time-space as $(\tilde{t}(\sigma), \tilde{x}(\sigma), \tilde{c}(\sigma))$. Extending the notation (A.6) to the 3-dimensional case and proceeding in the same way as in Appendix A, we obtain the characteristic system

$$\frac{d\tilde{t}(\sigma)}{d\sigma} = 1, \quad (\text{C.3a})$$

$$\frac{d\tilde{x}(\sigma)}{d\sigma} = \tilde{c}(\sigma), \quad (\text{C.3b})$$

$$\frac{d\tilde{c}(\sigma)}{d\sigma} = 0, \quad (\text{C.3c})$$

$$\frac{d\tilde{\xi}_w(\sigma)}{d\sigma} = -b(\tilde{t}(\sigma)) \tilde{\xi}_w(\sigma), \quad (\text{C.3d})$$

$$\frac{d\tilde{\xi}_d(\sigma)}{d\sigma} = 0. \quad (\text{C.3e})$$

The general solution of the ODEs (C.3) is

$$\tilde{t}(\sigma) = \tilde{t}(0) + \sigma, \quad (\text{C.4a})$$

$$\tilde{x}(\sigma) = \tilde{x}(0) + \tilde{c}(0)\sigma, \quad (\text{C.4b})$$

$$\tilde{c}(\sigma) = \tilde{c}(0), \quad (\text{C.4c})$$

$$\tilde{\xi}_w(\sigma) = \tilde{\xi}_w(0) \beta(\tilde{t}(0), \tilde{t}(\sigma)), \quad (\text{C.4d})$$

$$\tilde{\xi}_d(\sigma) = \tilde{\xi}_d(0) \quad (\text{C.4e})$$

where

$$\beta(t_1, t_2) := \exp\left(-\int_{t_1}^{t_2} b(\alpha) d\alpha\right). \quad (\text{C.5})$$

Similarly to the proof of Lemma 1 in Appendix A, two boundary conditions are imposed on the characteristic curve, the first being

$$\tilde{t}(\sigma) = t, \quad \tilde{x}(\sigma) = x, \quad \tilde{c}(\sigma) = c \quad (\text{C.6})$$

and with regards to the second boundary condition we distinguish two cases:

1. If $t_0 \leq t < t_0 + x/c$, then we take

$$\tilde{t}(0) = t_0, \quad \tilde{x}(0) = (x - (t - t_0)c) \in (0, x], \quad \tilde{c}(0) = c \quad (\text{C.7})$$

which yields the first part of solution (C.1).

2. If $t \geq t_0 + x/c$, then

$$\tilde{t}(0) = t - x/c \geq t_0, \quad \tilde{x}(0) = 0, \quad \tilde{c}(0) = c \quad (\text{C.8})$$

which yields, using the boundary conditions from the PDEs (26), the other part (C.2).

Note that the OPF model does not need any restrictions on the initial and input velocities beyond their smoothness, unlike the DPF where we imposed the constraints (6)–(8) to ensure that the characteristics never cross. Indeed, it can be easily seen that the OPF characteristic curves (C.4) cannot intersect unless they coincide. \square

Finally, the outputs of the PDEs (26) are obtained for $t \geq t_0 + \ell/c_{\min}$ from (C.2) as (31), and the total water mass M_w is calculated by substituting (C.2) into (29) which yields (32). Thus, Theorem 3 is established.

Appendix D. Proof of Theorem 4

Here we describe the proof of Theorem 4 concerned with the input-output relations for the OPF model with localized evaporation. In the following Lemma we derive the solution of the OPF equations (26) under the localized evaporation model (34)–(37). Thence, the input-output relations are obtained, proving the Theorem.

Lemma 4. Under the conditions of Theorem 4 the PDE system (26), (34)–(37) admits the classical solution given, for $t \in [t_0, t_0 + x/c]$, by

$$\frac{\xi_w(t, x, c)}{\xi_d(t, x, c)} = \Omega \left(\frac{\xi_{w,0}(X, c)}{\xi_{d,0}(X, c)} + 1, \frac{\phi_0(X, c) \varpi(t_0, t)}{\xi_{d,0}(X, c)} \right) \Big|_{X=x-(t-t_0)c} - 1, \quad (\text{D.1a})$$

$$\xi_d(t, x, c) = \xi_{d,0}(x - (t - t_0)c, c) \quad (\text{D.1b})$$

and, for $t \geq t_0 + x/c$, by

$$\frac{\xi_w(t, x, c)}{\xi_d(t, x, c)} = \Omega \left(\frac{1}{w_{i,T}(\theta)}, \frac{c \varpi(\theta, t)}{\dot{m}_{i,T}(\theta) w_{i,T}(\theta)} \right) \Big|_{\theta=t-x/c} - 1, \quad (\text{D.2a})$$

$$\xi_d(t, x, c) = f(c, \theta) \dot{m}_{i,T}(\theta) w_{i,T}(\theta) / c \Big|_{\theta=t-x/c}. \quad (\text{D.2b})$$

Here Ω is defined via the Lambert W -function as

$$\Omega(a, b) := \frac{k_1}{k_0} \left(W \left[\left(\frac{k_0}{k_1} a - 1 \right) \exp \left(\frac{k_0}{k_1} a - 1 - \frac{k_0^2}{k_1} b \right) \right] + 1 \right) \quad (\text{D.3})$$

and we use the abbreviation

$$\varpi(t_1, t_2) := \int_{t_1}^{t_2} p(\alpha) d\alpha. \quad (\text{D.4})$$

Proof. The PDEs (26) of OPF with localized evaporation model (34)–(37) are solved similarly to the case of water-proportional evaporation (Appendix C). The only difference is in the behavior of ξ_w and in the additional PDE (36) for ϕ . The corresponding characteristic equations for ξ_w and ϕ are

$$\frac{d\tilde{\xi}_w(\sigma)}{d\sigma} = -\tilde{\phi}(\sigma) \left(k_0 - k_1 \frac{\tilde{\xi}_d(\sigma)}{\tilde{\xi}_w(\sigma) + \tilde{\xi}_d(\sigma)} \right) p(\tilde{t}(\sigma)), \quad (\text{D.5a})$$

$$\frac{d\tilde{\phi}(\sigma)}{d\sigma} = 0. \quad (\text{D.5b})$$

To solve the system of characteristic equations, we introduce the new variable

$$\tilde{\omega}(\sigma) := \frac{\tilde{\xi}_w(\sigma)}{\tilde{\xi}_d(\sigma)} + 1 \quad (\text{D.6})$$

which satisfies the ODE

$$\frac{d\tilde{\omega}(\sigma)}{d\sigma} = -\frac{\tilde{\phi}(\sigma) p(\tilde{t}(\sigma))}{\tilde{\xi}_d(\sigma)} \frac{k_0 \tilde{\omega}(\sigma) - k_1}{\tilde{\omega}(\sigma)}. \quad (\text{D.7})$$

Solving it together with the rest of the system (C.3) yields the general solution

$$\tilde{\omega}(\sigma) = \Omega \left(\frac{\tilde{\xi}_w(0)}{\tilde{\xi}_d(0)} + 1, \frac{\tilde{\phi}(0)}{\tilde{\xi}_d(0)} \varpi(\tilde{t}(0), \tilde{t}(0) + \sigma) \right). \quad (\text{D.8})$$

To obtain the general solution of the PDEs, two boundary conditions are imposed on the characteristic curve, the first being

$$\tilde{t}(\sigma) = t, \quad \tilde{x}(\sigma) = x, \quad \tilde{c}(\sigma) = c \quad (\text{D.9})$$

and with regards to the second boundary condition we distinguish two cases:

1. If $t_0 \leq t < t_0 + x/c$, then we take

$$\tilde{t}(0) = t_0, \quad \tilde{x}(0) = x - (t - t_0)c \in (0, x], \quad \tilde{c}(0) = c \quad (\text{D.10})$$

which yields

$$\omega(t, x, c) = \Omega \left(\frac{\xi_{w,0}(\chi, c)}{\xi_{d,0}(\chi, c)} + 1, \frac{\phi_0(\chi, c) \varpi(t_0, t)}{\xi_{d,0}(\chi, c)} \right) \Big|_{\chi=x-(t-t_0)c} \quad (\text{D.11})$$

where $\omega(t, x, c)$ is connected to $\tilde{\omega}(\sigma)$ by the notation scheme (A.6). It leads to (D.1).

2. If $t \geq t_0 + x/c$, then

$$\tilde{t}(0) = t - x/c \geq t_0, \quad \tilde{x}(0) = 0, \quad \tilde{c}(0) = c \quad (\text{D.12})$$

which, using the boundary conditions from the PDEs (26), leads to (D.2).

This completes the proof of the Lemma. \square

The outputs of the OPF model (26) for $t \geq t_0 + \ell/c_{\min}$ are computed via (D.2) and found to be in the form (39). This finally proves Theorem 4.

References

- Åkesjö, A., 2018. Hydrodynamics and heat transfer in vertical falling films with smooth and modified heat-transfer surfaces: an experimental and numerical investigation. Department of Chemistry and Chemical Engineering, Chalmers University of Technology.
- Albert, C., Marschall, H., Bothe, D., 2014. Direct numerical simulation of interfacial mass transfer into falling films. *International Journal of Heat and Mass Transfer* 69, 343–357.
- Bandi, P., Modigell, M., Gro, S., Reusken, A., Zhang, L., Heng, Y., Marquardt, W., Mhamdi, A., 2018. On reduced modeling of mass transport in wavy falling films. *AIChE Journal* 64 (6), 2265–2276.
- Bojnour, F.M., Fanaei, M.A., Zohreie, H., 2015. Mathematical modelling and dynamic simulation of multi-effect falling-film evaporator for milk powder production. *Mathematical and Computer Modelling of Dynamical Systems* 21 (4), 336–358.
- Bresch-Pietri, D., Leroy, T., Petit, N., 2013. Control-oriented time-varying input-delayed temperature model for SI engine exhaust catalyst. In: 2013 American Control Conference. IEEE, pp. 2189–2195.
- Bresch-Pietri, D., Petit, N., 2016. Implicit integral equations for modeling systems with a transport delay. In: *Recent Results on Time-Delay Systems*. Springer, pp. 3–21.
- Cascetta, E., 2013. *Transportation systems engineering: theory and methods*. Springer Science & Business Media.
- Čičić, M., Johansson, K.H., 2018. Traffic regulation via individually controlled automated vehicles: a cell transmission model approach. In: 21st International Conference on Intelligent Transportation Systems (ITSC). IEEE, pp. 766–771.
- Courant, R., Hilbert, D., 1989. *Methods of Mathematical Physics, Vol. II. Partial Differential Equations*. Wiley.
- Craster, R., Matar, O., 2009. Dynamics and stability of thin liquid films. *Reviews of modern physics* 81 (3), 1131–1198.
- Daganzo, C.F., 1994. The cell transmission model: a dynamic representation of highway traffic consistent with the hydrodynamic theory. *Transportation Research Part B: Methodological* 28 (4), 269–287.
- Diagne, M., Couenne, F., Maschke, B., 2013. Mass transport equation with moving interface and its control as an input delay system. *IFAC Proceedings Volumes* 46 (3), 331–336.
- Díaz-Ovalle, C.O., González-Alatorre, G., Alvarado, J.F.J., 2017. Analysis of the dynamic response of falling-film evaporators considering fouling. *Food and Bioprocess Processing* 104, 124–136.
- Dobos, L., Jäschke, J., Abonyi, J., Skogestad, S., 2009. Dynamic model and control of heat exchanger networks for district heating. *Hungarian Journal of Industry and Chemistry* 37 (1), 37–49.
- Donaldson, A., Thimmaiah, A., 2016. Process modelling and optimization of design parameters in a falling film plate and frame evaporator. In: *Proceedings of the COMSOL Conference*, pp. 1–9.
- Evesque, S., Annaswamy, A., Niculescu, S., Dowling, A., 2003. Adaptive control of a class of time-delay systems. *Journal of Dynamic Systems, Measurement, and Control* 125 (2), 186–193.
- Getz, N., Marsden, J.E., 1995. A dynamic inverse for nonlinear maps. In: 34th Conference on Decision and Control, 4. IEEE, pp. 4218–4223.
- GEA Wiegand GmbH, 2016. *Evaporation Technology*.
- Grifoll, J., Gastó, J.M., Cohen, Y., 2005. Non-isothermal soil water transport and evaporation. *Advances in Water Resources* 28 (11), 1254–1266.
- Hofmann, J., Ponomarev, A., Hagenmeyer, V., Gröll, L., 2020. Transport models for liquid films (in German). at - *Automatisierungstechnik* 68 (8), 625–640.
- Hofmann, J., Ponomarev, A., Hagenmeyer, V., Gröll, L., 2021. Time-delay identification and validation of a liquid film transport model based on pilot plant experiments. Accepted for 11th IFAC Symposium on Advanced Control of Chemical Processes (ADCHEM2021), preprint available online.
- Holman, J.P., 1989. *Heat Transfer*. McGraw-Hill.
- Karafyllis, I., Krstic, M., 2014. On the relation of delay equations to first-order hyperbolic partial differential equations. *ESAIM: Control, Optimisation and Calculus of Variations* 20 (3), 894–923.
- Karafyllis, I., Krstic, M., 2020. Stability results for the continuity equation. *Systems & Control Letters* 135, 104594.
- Kharangate, C.R., Lee, H., Mudawar, I., 2015. Computational modeling of turbulent evaporating falling films. *International Journal of Heat and Mass Transfer* 81, 52–62.
- Kicsiny, R., 2014. New delay differential equation models for heating systems with pipes. *International Journal of Heat and Mass Transfer* 79, 807–815.
- Levenspiel, O., 1999. *Chemical reaction engineering*. *Industrial & Engineering Chemistry Research* 38 (11), 4140–4143.
- Lukach, Y.Y., Radchenko, L.B., Tananayiko, Y.M., 1972. Determination of the average thickness of a film of water during gravitation of flow along the exterior surface of vertical polymeric pipes. *International Chemical Engineering* 12, 517–519.
- Maidi, A., Diaf, M., Corriou, J.P., 2009. Boundary geometric control of a counter-current heat exchanger. *Journal of Process Control* 19 (2), 297–313.

- Martin, H., Gnielinski, V., Mewes, D., Steiner, D., Stephan, K., Schaber, K., Vortmeyer, D., Kabelac, S., 2002. VDI Wärmeatlas: Berechnungsblätter für den Wärmeübergang. Springer.
- Misra, C., Mishra, B.K., 1977. Miscible displacement of nitrate and chloride under field conditions 1. *Soil Science Society of America Journal* 41 (3), 496–499.
- Niemi, A.J., 1977. Residence time distributions of variable flow processes. *The International Journal of Applied Radiation and Isotopes* 28 (10-11), 855–860.
- Nusselt, W., 1916. Die Oberflächenkondensation des Wasserdampfs. *Zeitschrift des Vereins Deutscher Ingenieure* 60, 542–546.
- Paramalingam, S., 2004. Modelling, optimisation and control of a falling-film evaporator. Massey University, New Zealand.
- Polyanin, A.D., Zaitsev, V.F., 2016. Handbook of nonlinear partial differential equations. Chapman and Hall/CRC.
- Ponomarev, A., Hofmann, J., Grill, L., 2020. Characteristics-based Simulink implementation of first-order quasilinear partial differential equations. In: 10th International Conference on Simulation and Modeling Methodologies, Technologies and Applications (SIMULTECH), pp. 139–146. doi:10.5220/0009569001390146.
- Quaak, P., van Wijck, M.P.C.M., van Haren, J.J., 1994. Comparison of process identification and physical modelling for falling-film evaporators. *Food Control* 5 (2), 73–82.
- Rodriguez, D.F.N., Witrant, E., Sename, O., 2016. Control-oriented modeling of fluid networks: a time-delay approach. In: *Recent Results on Nonlinear Delay Control Systems*. Springer, pp. 275–289.
- Ruyer-Quil, C., Manneville, P., 2000. Improved modeling of flows down inclined planes. *The European Physical Journal B – Condensed Matter and Complex Systems* 15 (2), 357–369.
- Sarra, S.A., 2003. The method of characteristics with applications to conservation laws. *Journal of Online Mathematics and its Applications* 3, 1–16.
- Schwaer, C., Hofmann, J., Mühlfordt, M., Frank, A., Gröll, L., 2020. Modular simulation model for falling film evaporators with novel approach to manage dominant time-varying transport delays. *Computers & Chemical Engineering* 132, 106604.
- Stefanov, Z.I., Hoo, K.A., 2003. A distributed-parameter model of black liquor falling film evaporators. Part I. Modeling of a single plate. *Industrial & Engineering Chemistry Research* 42 (9), 1925–1937.
- Van Genuchten, M.T., 1982. Analytical solutions of the one-dimensional convective-dispersive solute transport equation. US Department of Agriculture, Agricultural Research Service.
- Winchester, J., 2000. Model based analysis of the operation and control of falling-film evaporators. Massey University, New Zealand.
- Winchester, J.A., Marsh, C., 1999. Dynamics and control of falling film evaporators with mechanical vapour recompression. *Chemical Engineering Research and Design* 77 (5), 357–371.
- Witrant, E., Niculescu, S.I., 2010. Modeling and control of large convective flows with time-delays. *Mathematics in Engineering, Science and Aerospace* 1 (2), 191–205.
- Zenger, K., Ylinen, R., 1994. Simulation of variable delays in material transport models. *Mathematics and computers in simulation* 37 (1), 57–72.
- Zhang, H.M., 1998. A theory of nonequilibrium traffic flow. *Transportation Research Part B: Methodological* 32 (7), 485–498.
- Zheng, C., Bennett, G.D., 2002. Applied contaminant transport modeling. Wiley-Interscience.
- Zhong, Q.-C., 2006. Robust control of time-delay systems. Springer Science & Business Media.

Repository KITopen

Dies ist ein Postprint/begutachtetes Manuskript.

Empfohlene Zitierung:

Ponomarev, A.; Hofmann, J.; Gröll, L.

[Novel Control-Oriented Models for Liquid Transport in Falling Film Evaporator Tubes.](#)

2021. Computers & chemical engineering, 152, Article no: 107376.

doi: [10.5445/IR/1000133230](https://doi.org/10.5445/IR/1000133230)

Zitierung der Originalveröffentlichung:

Ponomarev, A.; Hofmann, J.; Gröll, L.

[Novel Control-Oriented Models for Liquid Transport in Falling Film Evaporator Tubes.](#)

2021. Computers & chemical engineering, 152, Article no: 107376.

doi: [10.1016/j.compchemeng.2021.107376](https://doi.org/10.1016/j.compchemeng.2021.107376)

Lizenzinformationen: [CC BY-NC-ND 4.0](#)